Published in final edited form as:
Nature. 2022 April 01; 604(7905): 323–329. doi:10.1038/s41586-022-04546-y.

Two defence systems eliminate plasmids from 7th pandemic *Vibrio cholerae*

Milena Jaskólska[#1], **David W. Adams**[#1,*], **Melanie Blokesch**[1,*]

[1]Laboratory of Molecular Microbiology, Global Health Institute, School of Life Sciences, Station 19, EPFL-SV-UPBLO, Ecole Polytechnique Fédérale de Lausanne (EPFL), CH-1015 Lausanne, Switzerland

[#] These authors contributed equally to this work.

Abstract

Horizontal gene transfer (HGT) can trigger rapid shifts in bacterial evolution. Driven by a variety of mobile genetic elements, in particular bacteriophages and plasmids, the ability to share genes within and across species underpins the unparalleled adaptability of bacteria. Nevertheless, invasive mobile genetic elements can also present grave risks to the host, bacteria have therefore evolved a vast array of defences against these elements[1]. Here we identify two plasmid defence systems conserved in the *Vibrio cholerae* El Tor strains responsible for the ongoing 7[th] cholera pandemic[2–4]. These systems termed DdmABC and DdmDE, are encoded on two major pathogenicity islands that are a hallmark of current pandemic strains. We show that both modules co-operate to rapidly eliminate small multi-copy plasmids by degradation. Moreover, the DdmABC system is widespread and can defend against bacteriophage infection by triggering cell suicide (abortive infection; Abi). Remarkably, we go on to show that via an Abi-like mechanism DdmABC increases the burden of large low-copy number conjugative plasmids, including a broad-host IncC multidrug resistance plasmid, creating a fitness disadvantage that counter-selects against plasmid-carrying cells. Our results answer the long-standing question of why plasmids, while abundant in environmental strains, are rare in pandemic strains, have implications for understanding the dissemination of antibiotic resistance plasmids, and provide insights into how the interplay between two defence systems has shaped the evolution of the most successful lineage of pandemic *V. cholerae*.

Vibrio cholerae has been responsible for seven cholera pandemics, the latest of which remains ongoing[2]. It is caused primarily by strains of the O1 El Tor biotype (7PET), which have displaced those of the O1 classical biotype responsible for the 6th pandemic[3,4]. Most strains however are natural inhabitants of the aquatic environment, with only two serogroups

[*]For correspondence: david.adams@epfl.ch or melanie.blokesch@epfl.ch.

Author contributions

M.J., D.W.A. and M.B. conceived the project, designed the experiments, constructed strains and plasmids, and analysed the results. M.J. and D.W.A. performed all experiments in collaboration, except for phage assays, which were done by M.J, and microscopy, which was done by D.W.A. D.W.A performed bioinformatic analyses. D.W.A and M.J wrote the paper with input from M.B. M.B. acquired funding and supervised the project.

Competing interests

M.B, M.J, and D.W.A. are inventors on the patent application EP21183501.2 filed with the European Patent Office.

Europe PMC Funders Author Manuscripts

(O1/O139) capable of causing pandemic disease[3,4]. Fundamental to the transition from environmental resident to pandemic human pathogen has been the acquisition of a variety of genomic islands, including the cholera toxin prophage (CTXΦ)[5], the *Vibrio* pathogenicity islands (VPI-1/2)[6,7], and more recently, the *Vibrio* seventh pandemic islands (VSP-I/II), which are exclusive to the 7PET and define the switch from the 6th to 7th pandemic[4,8–10].

Thus, HGT has played a key role in the evolution of pandemic *V. cholerae*. But HGT can also pose grave risks. In addition to the immediate danger posed by lytic phage, some mobile genetic elements can act as parasites, or else carry integrative elements that can disrupt genomic integrity[11,12]. In response, bacteria have evolved a vast array of defence systems to counter this threat[1]. Plasmids, autonomously replicating extra-chromosomal DNA molecules, are common vehicles for HGT and are ubiquitous throughout the bacteria. Indeed, plasmids are abundant throughout the *Vibrionaceae*, including in environmental strains of *V. cholerae*[13–15]. However, they are conspicuously absent from most pandemic strains[16–19]. The vast majority of these strains lack known plasmid defence systems such as CRISPR-Cas and Argonaute[4,20,21]. We therefore hypothesised that additional mechanisms likely await discovery in the 7PET, and that they may have played a crucial role in the evolution and success of these strains.

Plasmids are unstable in O1 El Tor

To test this hypothesis, we first investigated plasmid stability in the representative 7PET strain A1552 during growth for approximately 50 generations with and without selection. Unexpectedly, the commonly used *Escherichia coli* ColE1/pMB1/pBR322/pUC-family plasmid pBAD/Myc-HisA (pBAD) proved to be highly unstable, resulting in gross morphological defects under selection, likely due to plasmid loss (Fig. 1a-b). Since this family of vectors is not native to *Vibrio sp*. we set out to identify a natural *V. cholerae* plasmid to use as a model. As expected, none were detected in the best-studied pandemic strains. In contrast, 5/15 strains from a collection of environmental isolates were found to contain a small cryptic plasmid (Extended Data Fig. 1a-b). Characterisation of these plasmids led to identification of pSa5Y, a 3.5kb plasmid present at 4-5 copies per genome, which replicates using a Marine RNA-based (MRB) origin of replication[13,14] (Extended Data Fig 1c-f; See Methods). Since MRB plasmids are prevalent throughout the *Vibrionaceae* and highly stable in their host species[13,14,22], we chose to use pSa5Y as a model plasmid. In contrast to pBAD, selectable pSa5Y derivatives were stable and well tolerated, but were still gradually lost in the absence of selection (Fig. 1a-b). Strikingly, when we re-evaluated plasmid stability in a diverse set of environmental, clinical and pandemic *V. cholerae* strains, pSa5Y was highly stable in all tested strains, except those of the O1 El Tor clade (Fig. 1c). This phenotype was not specific to pSa5Y since a neutral plasmid backbone containing various different origins of replication also behaved similarly (Fig. 1d).

Discovery of two DNA defence modules

The stability of pSa5Y in O139 strains was unexpected. These strains represent a discrete lineage of 7PET and are thought to have emerged after an O1 El Tor ancestor acquired

the O139-antigen-specific genes by HGT[23,24]. Indeed, simply serogroup-converting A1552 from O1 to O139 by natural transformation[24] had no effect on plasmid stability (Fig. 2a-b). However, O139 strains also carry a truncated version of VPI-2, a 57kb island that harbours a sialic-acid utilisation cluster, a restriction-modification (R/M) system, and a predicted phage defence system (Zorya)[7,25] (Fig. 2a). Strikingly, a partially serogroup-converted transformant that had co-transferred this deletion exhibits complete plasmid stabilisation (Fig. 2a-b). To determine which of the 28 missing genes is responsible for this phenotype, we performed a deletion series across VPI-2, followed by individual deletions and complementation assays (Fig. 2c-e). This revealed that the 2-gene operon VC1771-70 is required for plasmid destabilisation. Furthermore, while both genes could complement their respective individual deletions, neither was capable of complementing the whole region deletion, suggesting that they work together. Importantly, the role of this region in plasmid destabilisation is conserved in a representative set of 7PET strains (Extended Data Fig. 2a). However, VPI-2 is intact in the 6th pandemic classical strain O395, and the related O37 serogroup strain ATCC25872, both of which keep plasmids, and express VC1771-70 at similar levels to A1552 (Extended Data Fig. 2b), suggesting that additional genes are likely involved in plasmid destabilisation.

Defence systems are often enriched on genomic islands[25,26]. We therefore investigated the involvement of additional pathogenicity islands by deleting VPI-1, VSP-I and VSP-II (Fig. 2f). Strikingly, in the absence of VSP-II, a 27kb island of mostly unknown function[9], about 2/3 of cells now retained the plasmid (Fig. 2g-h). Following the same deletion and complementation approach outlined above we determined that the 3-gene operon VC0492-90 is required for plasmid destabilisation and that these genes likely work together (Fig. 2i-k). Interestingly, closer inspection of O395 and other classical strains examined, which lack VSP-II, revealed a common substitution (E891K) in VC1771 that impairs its function and renders its activity VC0492-90-dependent (Extended Data Fig. 2c-e), thus explaining why plasmids are stable in classical strains despite the presence of VC1771-70.

Plasmids carrying various origins of replication largely behaved similarly to pSa5Y in the absence of either VC1770 or VC0490, confirming that these phenotypes are not specific to the model plasmid. However, the p15A origin plasmid was stabilised only by the deletion of VC0490, suggesting that some degree of specificity is present. Indeed, the gross morphological defects associated with instability of the pBAD plasmid were also rescued specifically by the loss of VC0492-90 (Extended Data Fig. 2f-g). Finally, we found no evidence of regulatory cross-talk between the expression of the two operons (Extended Data Fig. 2h). Thus, both VC1771-70 (VPI-2) and VC0492-90 (VSP-II) are required for plasmid destabilisation in 7PET. Moreover, since deletion of VC1771-70 results in a near total loss of plasmid elimination, whereas the effect of VC0492-90 is intermediate, these data suggest a model whereby the two discrete systems work together, with VC0492-90 acting either to enhance VC1771-70 activity or else acting in a VC1771-70-dependent manner. Given these results, we propose to rename VC0492-90 and VC1771-70 to DNA-defence modules DdmABC and DdmDE, respectively.

DdmABC and DdmDE have distinct activities

To test this model, we created ectopically integrated arabinose-inducible versions of each operon (*i.e. TnddmABC* and *TnddmDE*), both of which could complement the deletion of their respective operons (Fig. 3a). In a double deletion background (Δ*ddm*), DdmDE production resulted in complete plasmid elimination. In contrast, although DdmABC also led to significant plasmid loss, this was incomplete. Thus, both systems can function independently when overexpressed. Next, using *E. coli* as a heterologous system, we tested for activity against a variety of plasmid origins (Fig. 3b). Notably, DdmDE production was sufficient to eliminate plasmids from most cells within only 10 generations, indicating that its activity is independent of the mode of plasmid replication. In contrast DdmABC production had no obvious effect on plasmid stability. Interestingly, however, in both organisms *TnddmABC* produced a strong growth defect under full induction, with swollen cells that often appeared to be either anucleate or have otherwise defective nucleoids (Extended Data Fig. 3a-c). Moreover, this toxicity was plasmid-dependent, and enhanced by the absence of DdmDE, suggesting that plasmid DNA (pDNA) renders DdmABC active against the host.

Since some defence systems can target both plasmids and bacteriophage[1,27], we challenged *E. coli* cells expressing each operon with a panel of five well-characterised coliphages. Remarkably, while DdmDE had no obvious effect, DdmABC production provided substantial protection against phages λ and P1, mediating a ≥4-log decrease in the efficiency of plaque formation (Fig. 3c). Given the plasmid-dependent toxicity observed with DdmABC, we hypothesised that phage protection might be mediated by abortive infection (Abi), a mechanism that by sacrificing infected individuals prior to the completion of phage replication, provides population level immunity[28]. To test this, we followed the kinetics of P1 infection, in the absence and presence of DdmABC production (Fig. 3d). At low multiplicity of infection (MOI), where only a subpopulation of cells is initially infected, DdmABC provided robust protection against phage-induced culture collapse. In contrast, at high MOI, where the majority of cells should be infected, DdmABC tiggered growth arrest and lysis at 30min, approximately 20min prior to the phage-induced lysis observed in the no-system control, demonstrating that DdmABC acts via Abi.

To further investigate Ddm activity in *V. cholerae* we visualised pSa5Y using a ParB^{MT1}/*parS*^{MT1} fluorescent labelling system[29]. Cells carrying pSa5Y-*parS*^{MT1} contained multiple highly mobile foci, consistent with pSa5Y being a low multi-copy number plasmid (Extended Data Fig. 4a, Supplementary Video 1). Quantification by microscopy and plating confirmed that labelling does not affect plasmid stability. Furthermore, although some plasmid loss was already apparent by 10 generations, the most prominent difference was that a subset of cells contained large plasmid clusters that were largely absent in Δ*ddmABC* (Extended Data Fig. 4b-f). Upon overexpression of either *ddmDE* or *ddmABC* in the presence of the other system, we observed rapid plasmid elimination within the same time-frame, though DdmABC was noticeably less efficient and cells retained bright plasmid clusters (Fig. 3e). Remarkably, DdmDE produced alone in the double deletion background remained highly efficient, whereas DdmABC production led to cells with abnormal morphologies, most of which retained plasmids in large static clusters (Fig. 3e,

Supplementary Video 2). Time-course experiments revealed that plasmid elimination by DdmDE was rapid, occurring within only a few generations, and was unaffected by blocking cell division, indicating that DdmDE likely degrades pDNA (Extended Data Fig. 5a). In contrast, DdmABC-dependent cluster formation occurred more slowly, and blocking cell division significantly enhanced plasmid-dependent toxicity, likely reflecting the inability to lose plasmids by dilution upon division (Extended Data Fig. 5b). Finally, none of the proteins individually displayed any activity in either plasmid elimination, clustering or phage defence (Extended Data Fig. 6a-d). Taken together, these data suggest that under physiological conditions, DdmDE eliminates plasmids by degrading them and that this process is enhanced by DdmABC.

Mechanistic insights into Ddm activity

The *ddm* operons are not part of a known defence system. Bioinformatic analysis of DdmD revealed an N-terminal helicase domain containing conserved residues involved in nucleotide binding and hydrolysis characteristic of superfamily 2 helicases[30], and a C-terminal domain containing a PD-(D/E)xK superfamily nuclease motif[31] (Fig. 3f, Extended Data Fig.7, Supplementary Tables 1-3). Variants designed to disrupt either ATP-binding (DdmD[K55A]) and hydrolysis (DdmD[E273A]) or nuclease activity (DdmD[K1102A]) all abolished plasmid elimination (Fig. 3g). These variants remained non-functional even when overproduced, although DdmD[K1102A] exhibited residual activity that was *ddmABC*-dependent, suggesting DdmABC can partially compensate for the loss of nuclease activity (Extended Data Fig. 8a-c). In contrast, structural modelling indicated a possible relationship between DdmE and prokaryotic Argonautes (pAgo), which typically act as nucleic acid guided endonucleases involved in defence[27,32]. However, DdmE was not identified in a recent comprehensive analysis of pAgos[21] and we were unable to detect canonical Argonaute domains (*e.g.* PIWI). Nevertheless, since pAgos are often catalytically inactive, instead functioning with a partner nuclease[21], one possibility is that DdmE functions as a pAgo-like DNA-sensor, with DdmD acting as the effector. Interestingly, two-gene operons encoding DdmDE homologues are found throughout the *Vibrionaceae* as well as in the *Lactobacillaceae* (Extended Data Fig. 9a-c).

Analysis of DdmABC revealed that DdmC is an SMC-like protein, with a characteristic globular head domain composed of N- and C-terminal nucleotide binding motifs, separated by a central coiled-coil arm[33] (Fig.3h, Extended Data Fig.7, Supplementary Tables 1-3). Structural Maintenance of Chromosomes (SMC) family proteins such as MukB form multi-subunit complexes with the non-SMC protein MukE and the kleisin MukF, and are required for proper chromosome organisation[33,34]. However, given its comparatively small size (653 aa), short coiled-coil region (*c.a.* 20 nm), and lack of a recognisable hinge or zinc-hook domain, DdmC more closely resembles RecN, an SMC-like protein involved in double-strand break repair[33,35]. Moreover, the Walker B motif sits within a domain of unknown function (DUF3732), and carries an atypical E to Q substitution, suggesting it may be defective[33,34]. Further distinguishing DdmABC from canonical SMC complexes, as well as the 4-gene Wadjet/MksBEFG anti-plasmid defence system that combines an SMC complex and a topoisomerase, is that it appears to lack direct equivalents of MukE and MukF[25,36,37]. Instead, DdmA is predicted to consist of an N-terminal Cap4 dsDNA

endonuclease domain, containing a PD-(D/E)xK superfamily nuclease motif[38], and a C-terminal domain of unknown function, while DdmB encodes a small protein with the DUF6521 (Fig. 3h, Extended Data Fig.7). Operons of similar organisation (multidomain protein with a predicted effector domain, a middle component, and an ATPase) have recently been classified as a novel clade of the ABC type ATPases, suggested to function in defence[39]. Variants designed to disrupt either DdmA nuclease activity (DdmA[K57A]) or DdmC ATP-binding (DdmC[K40A]) abolished plasmid elimination (Fig. 3i), and even when overproduced remained defective for plasmid-dependent clustering and toxicity, and efficient anti-phage activity (Fig. 3c, Extended Data Fig. 3a, 8d-f). Notably, three-gene operons encoding a DUF3732-containing DdmC-like protein are widespread throughout the Proteobacteria, and intriguingly, are found on plasmids of the *Rhizobiaceae* including the *Agrobacterium tumefaciens* tumour-inducing plasmid (Extended Data Fig. 9d-e).

Ecological relevance of Ddm systems

To further investigate the relevance of the Ddm systems to the ecology and evolution of *V. cholerae* we examined a collection of naturally occurring plasmids, ranging from small (<10kb) multi-copy number plasmids, to large low-copy conjugative plasmids (pSA7G1, 79.4kb; pW6G, 306.5kB; pVCR94, 171.8kb). Notably, pVCR94 is part of the IncC family of broad-host multi-drug resistance (MDR) plasmids that foster dissemination of antibiotic resistance in diverse Gram-negative pathogens[40,41], and are the only plasmids known to be stable in 7PET[16,19]. As expected, all small plasmids were unstable in a Ddm-dependent manner. However, the large plasmids appeared to be unaffected by Ddm (Fig. 4a). Next, we tested whether Ddm affects plasmid acquisition. While we observed no meaningful differences on plasmid acquisition by natural transformation, acquisition by either electroporation or conjugation was increased in the absence of *ddmABC* (Extended Data Fig. 10a-c). This was especially clear for the large plasmids, with a 5-20 fold increase in transfer, although for pSA7G1, DdmABC and DdmDE had an additive effect (Fig. 4b). Thus, both systems can also reduce the acquisition of plasmids in 7PET.

Using pVCR94, we further investigated large plasmid stability. Genes implicated in plasmid stabilisation or host defence evasion[42,43] mostly proved dispensable, though we were unable to delete *parAB* (Extended Data Fig. 10d). Likewise, pVCR94 does not globally inactivate Ddm activity, since its presence had no effect on pSa5Y elimination (Extended Data Fig. 10e). In contrast, full induction of Tn*ddmABC* resulted in significant plasmid elimination and was accompanied by a clear plasmid-dependent growth defect (Extended Data Fig. 10f-g). Given that DdmABC can act against the host upon sensing plasmids or phage, we hypothesised that at physiological levels, plasmid recognition by DdmABC might generate a subtle but continuous growth defect, which may lead to strains being outcompeted by non-burdened plasmid-free cells. To test this, we competed plasmid-free WT cells with either WT or Δ*ddm* carrying the large plasmids pW6G and pVCR94, which both appear to be targeted specifically by DdmABC, revealing that plasmid-carrying cells exhibit a substantial Ddm-dependent competitive defect. As predicted, time-course experiments showed that this results from a small defect that gradually accumulates over time (Extended Data Fig. 10h-i). Moreover, individual deletions confirmed that this phenotype was DdmABC-dependent (Fig. 4c). Interestingly, although Δ*ddm* greatly relieved the fitness defect, it was not complete,

indicating that the plasmids themselves likely impart a burden. Thus, in the absence of selection, DdmABC removes large plasmids from the population by creating an enhanced fitness-cost that favours plasmid-free cells.

Widespread antibiotic use during African cholera epidemics has been linked to the proliferation of IncC MDR plasmids[19]. Given their stability and efficient spread by conjugation, these plasmids would be predicted to be maintained. However, these strains have largely been displaced by Asian isolates carrying SXT/R391 family integrative conjugative elements (ICE)[44], which globally are now the dominant form of MDR in *V. cholerae*[19]. Given the DdmABC-dependent burden faced by plasmid-carrying cells, we hypothesised that ICE-containing strains would likely have a fitness advantage. Indeed, competition experiments using A1552 derivatives containing two different ICEs (SXT and *Vch*Ind5[44]), revealed that although the ICE themselves impart a cost, this was significantly lower than with pVCR94 (Extended Data Fig. 10j). Furthermore, both ICE-carrying strains tested outcompeted pVCR94-containing cells (Fig. 4d), demonstrating that the DdmABC-enhanced burden of plasmid carriage may have contributed to the switch from large MDR plasmids to ICE.

Discussion

The principal finding of this work is the discovery of the Ddm systems in 7PET and that they can work together or independently to defend against plasmids and bacteriophages (Extended Data Fig. 10k). DdmDE eliminates small plasmids by degradation. DdmABC enhances this activity, either by clustering plasmids and/or directly participating in their degradation. In contrast, by targeting the infected host DdmABC defends the population against bacteriophage infection by a classical Abi mechanism. Remarkably, DdmABC also eliminates large conjugative plasmids via a similar Abi-like mechanism that counter-selects against plasmid-carrying cells. Thus, the combined activity of the Ddm systems provides a compelling explanation to why plasmids are largely absent from 7PET.

How ‘foreign’ DNA is discriminated remains unclear. An attractive possibility is that DdmE acts as a pAgo-like DNA-sensor to direct DdmD helicase-nuclease activity. Indeed, pAgos have been shown to preferentially form guides targeting plasmids based on their multi-copy nature and lack of Chi sites compared to chromosomal DNA[27,32]. In contrast, DdmABC toxicity is activated by the presence of non-self DNA. Interestingly, the Cap4 nuclease domain present in DdmA was shown to be a promiscuous nuclease[38], which in cyclic oligonucleotide-based anti-phage signalling systems (CBASS) is maintained as an inactive monomer until ligand-induced oligomerisation[38,45]. Since DdmA lacks the oligonucleotide-sensing SAVED domain[38], we propose that nuclease activity is coupled directly to DNA-sensing by the SMC-like protein DdmC. Indeed, upon recruitment to DNA SMC family proteins form oligomeric structures and can distinguish between various DNA features such as size, topology and damage[33,34]. Notably, diverse host defence systems utilise SMC-like proteins (SMC5/6[46], Wadjet/MksBEFG[25,37], Lamassu[25]), suggesting that their inherent ability to act as DNA-sensors has been exploited multiple times throughout evolution. Given that DdmABC homologues appear to be widespread, we propose that the DUF3732 present in DdmC may define a new family of SMC-like proteins dedicated to defence.

Pandemic strains of *V. cholerae* are adapted to a life-cycle centred on the human host. Thus, the ability to reduce the carriage of undomesticated plasmids that can impart an immediate growth defect, defend against bacteriophage, and possibly also eliminate temperate phage that propagate as plasmids, all have clear potential evolutionary benefits for maintaining the fitness of these strains[11,12,15]. Nevertheless, future work will still be required to distinguish between the beneficial consequences of Ddm activity and the factors driving their evolution, especially given that although DdmABC provides population level protection, it is costly to individual cells. Interestingly, by reducing both the acquisition and accelerating the purification of plasmid-carrying cells from the population, systems such as DdmABC can defend against the persistence of parasitic plasmids, which can persist without selection due to high rates of conjugation or adaptation[11,47]. However, another consequence of DdmABC activity is that beneficial plasmids will only be maintained through selection. This has important implications for understanding the dissemination of antibiotic resistance plasmids[47]. Indeed, this may have contributed to the failure of IncC plasmids to persist in the 7PET, with MDR now primarily encoded by SXT-like ICE[19], which interestingly, also harbour anti-phage defence systems[48]. Finally, the ability of DdmABC to act as a dual-function Abi system, targeting both phage and plasmids, raises the prospect that other Abi systems may also have roles beyond phage defence, as has recently been proposed[49].

In conclusion, VPI-2 appears to be a canonical defence island, with three distinct defence systems (Zorya, R/M, DdmDE) clustered together. Moreover, although the VSP islands are thought to have played a key role in the success of 7PET[8,10], until recently their role had remained unclear. Indeed, even though relatively small, VSP-I (14kb) has been shown to contain two separate phage defence systems, comprising the DncV-CapV CBASS[45,50,51] and DcdV[52] systems. Furthermore, we show here that VSP-II harbours the multi-purpose plasmid/bacteriophage defence module DdmABC, and that its role in defence against small plasmids is functionally coupled to VPI-2. Importantly, although VSP-II exists in several different configurations[19,53], many bearing large deletions, a recent survey of 1070 7PET isolates showed that *ddmABC* remains highly conserved[19]. We therefore propose that the combined capabilities of these islands to defend against various MGEs has played a key role in the evolution of 7PET, likely contributing to the displacement of the 6th pandemic strains that lack these mechanisms, and thus its emergence as the most successful lineage of pandemic *V. cholerae* to date.

Methods

Bacterial strains

The bacterial strains used in this study are listed in Supplementary Table 4. A1552, the primary *V. cholerae* 7PET strain used throughout this work is a fully sequenced toxigenic O1 El Tor (Inaba) representative of the on-going 7th cholera pandemic[54]. Experiments in *E. coli* were performed using the *E. coli* K-12 strain MG1655. Cloning was done using *E. coli* strains DH5α, TOP10, and where appropriate, strains S17-1λ*pir* and MFD*pir* were used for the propagation of plasmids with the conditional R6K origin of replication and for bacterial mating.

Growth conditions

Bacteria were cultured either in Lysogeny Broth (LB-Miller; 10 g/l NaCl, Carl Roth, Switzerland) with shaking at 180 rpm or on LB agar plates, at 30°C or 37°C, as required. Where appropriate, antibiotic selection was done with ampicillin (Amp, 50 or 100 μg/ml), kanamycin (Kan, 75 μg/ml for *V. cholerae;* 50 μg/ml for *E. coli*), gentamicin (Gent, 50 μg/ml), streptomycin (Strep, 100 μg/ml), rifampicin (Rif, 100 μg/ml), zeocin (Zeo, 100 μg/ml), erythromycin (Erm, 25 μg/ml) and nalidixic acid (Nx, 40 μg/ml). Counter-selection of *E. coli* following mating into *V. cholerae* was performed using thiosulfate citrate bile salts sucrose (TCBS; Sigma-Aldrich) agar supplemented with appropriate antibiotics. Mating with MFD*pir* derivatives to introduce the mini-Tn7 transposon into *E. coli* strain MG1655 was performed on agar supplemented with 0.3 mM diaminopimelic acid (DAP; Sigma-Aldrich) followed by selection of transconjugants on agar supplemented with gentamicin. SacB-based counter-selection was done on NaCl-free media supplemented with 10% sucrose. For strain construction by natural transformation, *V. cholerae* was grown on chitin flakes in 0.5x defined artificial seawater (DASW) supplemented with 50 mM HEPES and vitamins (MEM, Gibco), as previously described[55,56]. To induce expression from the P_{BAD} promoter growth media were supplemented with L-arabinose to a final concentration of either 0.02% or 0.2%, as indicated. To inhibit cell division in *V. cholerae*, cells were cultured with cephalexin (5 μg/ml).

Strain construction

DNA manipulations and molecular cloning were performed using standard methods[57]. Genetic engineering of *V. cholerae* was done using either natural transformation and FLP-recombination (TransFLP)[55,58,59] or by allelic exchange using the counter-selectable plasmid pGP704-Sac28 delivered via bi-parental mating from *E. coli*, as previously described[60]. All constructs were verified by colony PCR and Sanger sequencing (Microsynth AG, Switzerland), and analysed using SnapGene Ver. 4.3.11. A mini-Tn7 transposon carrying *araC* and the gene(s) of interest under control of the P_{BAD} promoter was integrated into a neutral chromosomal locus downstream of *glmS* in *V. cholerae* and *E. coli* by tri-parental mating, as previously described[61].

Plasmid construction

The plasmids used and constructed in this study are described in Supplementary Table 5. All inserted fragments were verified by sequencing (Microsynth AG, Switzerland). To test the stability of plasmids using different replicons, various origins of replication were cloned into a neutral plasmid backbone (pMJ174) containing the conditional R6K*ori* that is inactive in the tested strains (Supplementary Table 5). The primers used for cloning the origins of replication of various plasmids are listed in Supplementary Table 6. For plasmids pSa5Y, pE7G2, pSA7G1, and pW6G a kanamycin resistance cassette was introduced by natural transformation on chitin in the native plasmid-carrying strains, using a PCR fragment containing the kanamycin resistance gene flanked by sequences homologous to the respective plasmid. Plasmid DNA was isolated using either a GenElute HP Plasmid Miniprep Kit (Sigma-Aldrich) or a PureYield™ Plasmid Miniprep System (Promega). Where required, plasmids were introduced into electro-competent cells of *V. cholerae* by

electroporation at 1.6 kV and into chemically competent cells of *E. coli* using a standard heat shock protocol. Large, conjugative plasmids were transferred to *V. cholerae* recipients by mating on agar plates with a donor *E. coli* strain carrying the plasmid.

Sequencing of plasmids

The sequence of pSa5Y was initially obtained from a preliminary genome sequence of strain Sa5Y, and was subsequently confirmed by Sanger sequencing. Plasmids pSL4G and pSO5Y, from strains SL4G and SO5Y, were identified as pSa5Y-like by PCR and were sequenced using the same primers as for pSa5Y. To obtain the sequence of the two non-pSa5Y-like plasmids pSA7G3 and pE7G2, from strains SA7G and E7G, plasmid DNA was digested with *Eco*RV, 5'end phosphate groups were removed with Calf Intestinal Alkaline Phosphatase (New England Biolabs), and the linearised fragments inserted into the pCR-Blunt II-TOPO™ vector (Thermo Fisher Scientific). Plasmid DNA from positive clones was isolated and the inserted fragments sequenced using vector-specific primers. The remainder of the plasmids were sequenced with primers annealing to the regions identified in the first round.

Characterisation of pSa5Y and identification of the origin of replication

Plasmid pSa5Y (3494bp) was isolated from strain Sa5Y, which is part of a collection of Californian environmental *V. cholerae* isolates[62]. Quantitative PCR (qPCR) showed it is present at *c.a.* 4-5 copies per genome (Extended Data Fig. 1c). It carries 5 open reading frames of unknown function, including a gene encoding a putative adhesin, is non-conjugative and lacks a recognisable origin of transfer. Notably, characteristic genes involved in plasmid maintenance and partitioning such as toxin-antitoxin or *parAB* are also absent, and it could readily be cured (see below). BLAST-N analysis of the full-length pSa5Y sequence (3494 bp) was used to probe for conserved regions that could be indicative of an origin of replication. A ~500 bp region of pSa5Y was found to be widely conserved in plasmids of the *Vibrionaceae*, including numerous known members of the Marine RNA-based (MRB) plasmid family, which uses an RNA primer to initiate replication and an anti-sense RNA to control copy number[13,14]. Comparison of this region with the minimal origin region of the prototype MRB plasmid pB1067 from *Vibrio nigripulchritudo*[13] revealed a high degree of sequence identity (79%), as well as sequences encoding equivalents of the RNA I and RNA II species required for proper origin function (Extended data Fig. 1d-e). The functionality of the identified origin region was confirmed by its ability to impart *pir*-independent replication to an otherwise conditionally replicating plasmid containing the *pir*-dependent R6K origin of replication (Extended data Fig. 1f).

pSa5Y curing

pSa5Y was cured from strain Sa5Y by integrating a counter-selectable allele of the α subunit of phenylalanyl-tRNA synthetase, *pheS**[A294G/T251A], which renders cells sensitive to 4-chloro-phenylalanine (c-Phe; Sigma Aldrich)[63,64]. Briefly, a PCR fragment containing FRT-*aph-pheS**-FRT as well as flanking regions homologous to sequences on either side of the adhesin gene was integrated into pSa5Y in its native strain by natural transformation on chitin. An overnight culture of the resulting strain was diluted 10-fold, spread on LB plates containing 20 mM c-Phe, and incubated overnight at 30°C. The

resulting colonies were screened for kanamycin sensitivity and the loss of pSa5Y was confirmed by PCR with plasmid-specific primers and by agarose gel electrophoresis of plasmid DNA extractions.

Plasmid copy number

The copy number of pSa5Y was determined by quantitative PCR (qPCR) using the ratio of plasmid-specific amplification to the amplification of a genome-specific fragment, as previously described[65]. Cultures of strain Sa5Y were grown to either exponential ($O.D._{600}$ ~ 0.4-0.5) or stationary phase (overnight culture) and total DNA extracted using the DNeasy Blood and Tissue Kit (Qiagen) according to manufacturer's instructions. DNA was diluted to a concentration of 1 ng/μl and used for qPCR runs (LightCycler Nano, Roche) with primer pairs annealing within the plasmid and to the genomic *gyrA* sequence. The standard curve was prepared using a serial dilution (10^3–10^7 copies/μl) of the calibrator plasmid pCal-Sa5Y-1, which contains cloned fragments of the regions of pSa5Y and *gyrA* (1:1 amplified fragment ratio) used as targets for qPCR.

Plasmid stability assay

Plasmid stability assays were done using the indicated plasmids. For pSa5Y stability, the Amp^R and Kan^R derivatives, pSa5Y-Amp and pSa5Y-Kan were used interchangeably, as needed. Overnight cultures grown in the presence of antibiotic selection (designated as generation 0) were back-diluted to an $O.D._{600}$ of ~ 0.0025 in fresh LB medium, in the absence and presence of selection, as indicated, and grown with shaking at 30°C for approximately 10 generations, as estimated by optical density. To achieve growth for approximately 50 generations, cultures were back-diluted every 10 generations. At the desired end-point, cultures were serially diluted in PBS (phosphate buffered saline), spread on non-selective LB agar plates, and grown overnight at 30°C. The next day, 100 colonies were picked at random, patched onto selective media containing the appropriate antibiotic, and grown overnight at 30°C. Plasmid stability was calculated as the percentage of antibiotic resistant (*i.e.* plasmid-carrying) clones.

Quantitative Reverse Transcription PCR (qRT-PCR)

Overnight cultures were back-diluted 1:100 in LB medium and grown at 30°C with agitation for 3 h. RNA purification, cDNA synthesis and quantitative PCR were performed as previously described[66]. A LightCycler Nano was used for qPCR runs. Transcript levels in the graphs are presented as relative to the mRNA levels of the reference gene *gyrA*. The data were analysed with the LightCycler Nano software package v. 1.1.0 (Roche) using the standard curve method.

Bacteriophage plaque assay

The *E. coli* phages used in this study are listed in Supplementary Table 7 and were obtained as active cultures from the German Collection of Microorganisms and Cell Cultures (DSMZ). Overnight cultures of prey *E. coli* strains were back-diluted 1:100 in LB medium supplemented with 0.2% arabinose and grown at 37°C with shaking for 2 h. Exponentially growing cultures were then diluted 1:40 in a molten top agar (LB + 0.5% agar supplemented

with 5 mM $CaCl_2$, 5 mM $MgCl_2$ and arabinose), poured on top of a bottom layer of pre-solidified LB + 1.5% agar, and allowed to dry for 1 h. Phage were serially diluted in LB + 5 mM $CaCl_2$, 5 mM $MgCl_2$ and 5 μl of each of the dilutions spotted onto the seeded plates. Plates were imaged after incubation overnight (~ 16-18 h) at 37°C. Fold protection was calculated as the ratio of the number of plaques for the no system control (Tn-empty) to the number of plaques for strains expressing either *ddmDE*, *ddmABC*, or the various variants and individual components of DdmABC, and is expressed as the mean of three independent biological repeats. For representative examples of each plaque assay, see Supplementary Figure 1.

P1 infection kinetics

To follow the dynamics of P1 infection, overnight cultures of prey *E. coli* strains were back-diluted 1:100 in LB medium supplemented with 0.2% arabinose and grown at 37°C with shaking for 2 h. Cultures were then diluted 1:10 into LB supplemented with 5 mM $CaCl_2$ + 5 mM $MgCl_2$ + 0.2% arabinose. 180 μl of the diluted cultures were then added to wells of a 96-well plate containing 20 μl of phage P1 at multiplicity of infection (MOI) 0, 0.2 and 10 (in technical triplicate). Bacterial growth at 37°C with shaking was followed using a SpectraMax® i3x (Molecular Devices, USA) plate reader at 6 min intervals for a total of 49 cycles.

Concentrated P1 phage lysates were prepared by infecting exponentially growing cells of *E. coli* strain MG1655 at 37°C with phage P1 in LB medium supplemented with 5 mM $CaCl_2$ and 10 mM $MgCl_2$. Following almost complete lysis of the culture (3.5 h), lysates were centrifuged, passed through a 0.2 μm filter and chloroform added to a final concentration of 1% to prevent bacterial growth. Phage titres (pfu/ml) were determined on plates seeded with strain MG1655. To calculate the MOI, cultures of strains MG1655-Tn-empty and MG1655-Tn*ddmABC* were grown exactly as described in the assay above and colony forming units (cfu/ml) determined by spotting serially diluted cultures on LB plates, and are the mean of three independent biological repeats.

Microscopy

Cells were immobilised on slides coated with 1.2% w/v agarose in PBS, covered with a N°1 coverslip and examined using a Zeiss Axio Imager M2 epi-fluorescence microscope attached to an AxioCam MRm camera, controlled by Zeiss Zen software (ZEN 2.6 blue edition). Images were acquired using a Plan-Apochromat 100×/1.4 Ph3 oil objective illuminated by an HXP120 lamp, and were analysed and prepared for publication using ImageJ (Ver 2.1.0/1.53h; http://rsb.info.nih.gov/ij). To stain bacterial nucleoids, cultures were incubated with 4',6-Diamidino-2-phenylindole dihydrochloride (DAPI; Sigma Aldrich) at 5 μg/ml for 30 min at RT, before being washed once with PBS.

Plasmid labelling and quantification

Plasmids were visualised by a ParB-*parS* labelling approach[29], using strains constitutively producing yGFP-pMT1Δ23ParB and carrying pSa5Y-Kan variants harbouring the pMT1 *parS* site. Briefly, the *lacZ* region of the *V. cholerae* E7946 strain TND1379 (Δ*lacZ*::P_{lac}-CFP-$parB^{P1}$, yGFP-$parB^{MT1}$ Zeo^R)[67] was amplified by PCR and moved into *V. cholerae*

A1552 by natural transformation. A pair of oligonucleotides harbouring a 148 bp fragment containing the pMT1 *parS* site was used to introduce the *parS* site into pSa5Y-Kan by inverse PCR. To verify that ParB labelling did not affect plasmid stability, cultures were grown overnight with selection before being back-diluted to $O.D._{600}$ ~ 0.0025 in fresh media and grown for approximately 50 generations without selection. Cells were then processed for plasmid stability determination by plating, as described above, as well as being examined directly by fluorescence microscopy. To quantify plasmid stability, approximately 1600 cells were counted per strain, per condition, per repeat, and manually scored as either plasmid positive (≥1 yGFP-$ParB^{MT1}$ focus) or plasmid negative (yGFP-$ParB^{MT1}$ diffuse). To examine the effect of DdmDE and DdmABC overproduction on plasmid localisation and stability, cells were imaged after growth without selection for approximately 10 generations, in the absence and presence of inducer, as indicated. Plasmid stability was determined by microscopy, as described above, by counting approximately 700 cells per strain, per condition, per repeat.

Bioinformatics analysis

Sequence similarity searches were done with BLAST-P and with the PHMMER tool of the HMMER webserver version 2.41.1 (ebi.ac.uk/Tools/hmmer/) using the ensemblgenomes (v.44) database (http://ensemblgenomes.org), accessed in October 2020[68,69]. Remote homology detection was done with the HHpred server using PDB_mmCIF70_Oct14 as the target database (toolkit.tuebingen.mpg.de/tools/hhpred), accessed in October 2020[70,71]. Structural similarity prediction was done using a combination of the Phyre2.0[72] (sbg.bio.ic.ac.uk/phyre2) and i-TASSER[73] (zhanglab.ccmb.med.umich.edu/I-TASSER) webservers, using the default settings. Structural modelling was done using a combination of the RoseTTAFold[74] webserver and the ColabFold[75] implementation of AlphaFold2[76] using the default settings, and the resulting models used as templates for structural alignments done with PDBe Fold v2.59 (ebi.ac.uk/msd-srv/ssm/ssmstart.html). Additional conserved domains were identified using Pfam 34.0 (pfam.xfam.org). The predicted coiled-coil region of DdmC was further corroborated using Paircoil2[77]. To predict the presence of an origin of transfer site (*oriT*) plasmid DNA sequences were analysed using the OriTfinder[78] webserver (bioinfo-mml.sjtu.edu.cn/oriTfinder/).

Western blotting

Overnight cultures were back-diluted 1:100 and grown at 30°C with shaking for 3 h in LB supplemented with 0.02% or 0.2% of arabinose, as indicated. Lysates were prepared by suspending harvested cells in 2× Laemmli buffer (Sigma-Aldrich), normalised to optical density (100 μL buffer per O.D. unit) and incubated at 95°C for 15 min. Proteins were resolved on 10% Mini-PROTEAN TGX Stain-Free Precast gels and transferred onto PVDF membranes using a Trans-Blot Turbo Transfer System (Bio-Rad), according to the manufacturer's instructions. Membranes were then blocked at RT with agitation for 2 h in 3% skimmed milk in TBST (1×Tris-buffered saline with 0.1% Tween-20), the appropriate primary antibody was then added at a dilution of 1:1,000 and membranes were incubated at 4°C overnight. Membranes were then washed three times with TBST before incubation at RT for 1 h with Anti-Rabbit IgG (whole molecule)–Peroxidase (A9169; Sigma-Aldrich), diluted 1:10,000 in 3% skimmed milk in TBST. Membranes were washed

as above, and visualised by chemiluminescence using Lumi-Light^{PLUS} Western Blotting Substrate (Roche). Primary antibodies against DdmA (#2012839), DdmC (#2012829), DdmD (#2012831) and DdmE (#2012834) were custom-raised in rabbits against synthetic peptides (Eurogentec), and their specificity validated by the inclusion of samples from strains deleted for the appropriate genes. Uniform sample loading was verified by the intensity of non-specific bands on the membranes. For gel source data, see Supplementary Figure 1.

Conjugation assays

To render pSa5Y mobilizable by conjugation, the RP4 origin of transfer sequence (*oriT*) was amplified from pGP704 and cloned into pSa5Y-Kan. *E. coli* strain MFD*pir* containing the RP4 conjugation machinery served as the donor for pSa5Y-*oriT* transfer. Overnight cultures of the donor and recipients were harvested, washed once with PBS and concentrated 20-fold. Donor and recipient strains were mixed 1:1 and mating performed on LB plates supplemented with 0.3 mM DAP at 37°C for 6 h. For the mating of the large conjugative plasmids pSA7G1, pW6G and pVCR94 overnight cultures were back-diluted 1:100 into fresh LB medium with antibiotic selection and grown at 30°C for 3 h. Cultures were then harvested, washed once with PBS and concentrated 40-fold. Donor *E. coli* (MG1655 with streptomycin or nalidixic acid resistance) and recipient strains were mixed 1:1 and mating performed on tryptic soy agar (TSA) plates at 30°C for 6 h. Following mating, bacteria were collected, serially diluted and spotted on appropriate selective plates to enumerate exconjugants, recipients and donors. Transfer frequencies represent the ratio of exconjugants to the number of recipient cells, and are expressed as the mean of three independent biological repeats.

Plasmid transformation assays

Transformation frequencies with plasmid DNA were determined by either natural transformation on chitin or artificial introduction of the plasmid by electroporation. For natural transformation assays, overnight cultures were harvested, adjusted to O.D.$_{600}$ of 0.1 in 1ml 0.5× defined artificial seawater (DASW) supplemented with 50 mM HEPES and vitamins (MEM, Gibco) containing ~ 50-80 mg of chitin flakes (Sigma-Aldrich), and incubated statically at 30°C for 24h prior to the addition of pDNA (2 μg). After incubation at 30°C for a further 24 h, cells were detached from chitin flakes by vortexing, serially diluted in PBS and appropriate dilutions spread on LB plates with and without kanamycin.

For electroporation assays, overnight cultures were back-diluted 1:100 in LB medium and grown at 30°C with shaking for 3 h to O.D.$_{600}$ ~ 1. Cells were harvested, washed twice with ice-cold 2 mM $CaCl_2$, once with ice-cold 10% glycerol and the pellets resuspended in ice-cold 10% glycerol. Aliquots of 50 μl were flash frozen in a dry ice-ethanol bath and stored at -80°C for 24 h. Aliquots of electro-competent cells were thawed on ice, 300 ng of pSa5Y-Kan added and electroporation performed at 1.6 kV. Following electroporation, 2×YT medium was added to 1 ml and samples incubated statically at 37°C for 3 h, before being serially diluted in PBS and appropriate dilutions spread on LB plates with and without kanamycin. For both assays transformation frequency was calculated as the number of

kanamycin-resistant transformants divided by the total number of bacteria, and is expressed as the mean of three independent biological repeats.

Bacterial competition assays

The competitive index of strains carrying large plasmids or ICEs was determined in co-culture experiments using either A1552Δ*lacZ* (WT) or A1552Δ*lacZ* carrying the IncC plasmid pVCR94 (pVCR94) as reference strains. Overnight cultures of the test and reference strains were normalised according to optical density, mixed 1:1, back-diluted to an $O.D._{600}$ of ~ 0.0025 in fresh LB, and grown in the absence of antibiotic selection for approx. 10, 20, 30, 40 or 50 generations, as indicated, exactly as described for the plasmid stability assay. At the indicated time-points, cultures were then serially diluted in PBS and spread on LB agar plates supplemented with 5-Bromo-4-Chloro-3-Indolyl β-D-Galactopyranoside (X-gal; 40 μg/ml) and Isopropyl β-D-1-thiogalactopyranoside (IPTG; 1 mM). The fraction of blue (tested strain) and white (reference strain) colonies was enumerated following incubation at 37°C overnight (~ 18 h). The competitive index was calculated as the ratio of blue to white colonies divided by the ratio of the two strains in the starting inoculum and is expressed as the mean of three independent biological repeats.

Statistics and Reproducibility

All experimental data are representative of the results of three independent biological repeats. All replication attempts were successful. Statistical analysis was done using GraphPad Prism 9.1.2 (GraphPad Software, Inc., CA, USA). Significant differences were determined by one-way analysis of variance (ANOVA), and corrected for multiple comparisons using either Dunnett's or Tukey's post-test, as appropriate. The significance level (α) was set to 0.05 in all cases. For transformation frequency and transfer frequency experiments, analyses were performed on log-transformed data. The exact *P* values for all statistical comparisons are listed in Supplementary Table 8.

Europe PMC Funders Author Manuscripts

Europe PMC Funders Author Manuscripts

Extended Data

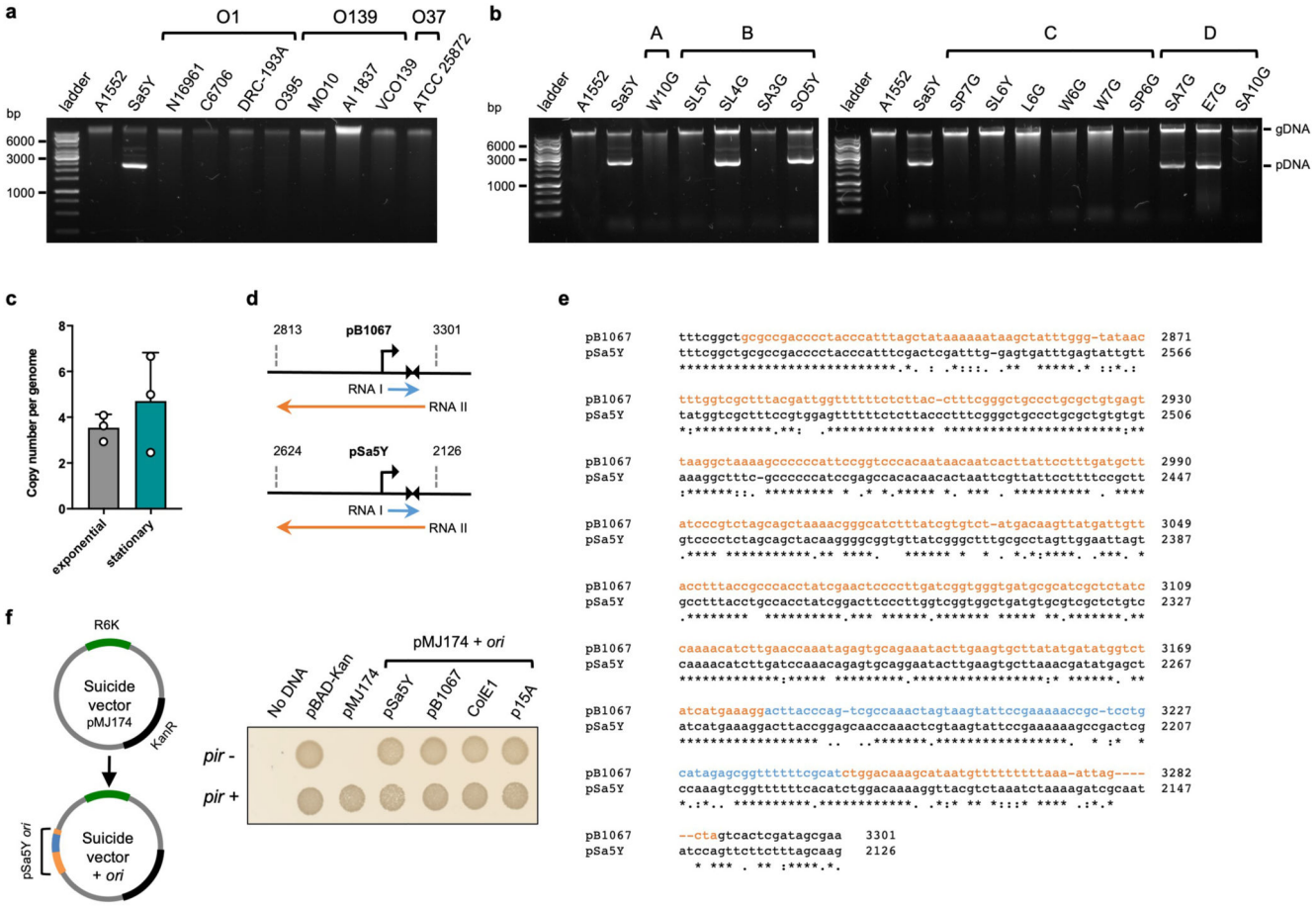

Extended Data Fig. 1. Characterisation of plasmids from an environmental Californian *V. cholerae* population.

a-b, Agarose gels showing plasmid DNA preparations from either a collection of pandemic and clinical strains with environmental strain Sa5Y as control (**a**) or the environmental non-O1/non-O139 Californian *V. cholerae* isolates (**b**). The letters above the gels in (**b**) denote the phylogenetic clade based on comparative genome hybridization[62]. gDNA, genomic DNA; pDNA, plasmid DNA. Strains SL4G and SO5Y contain a pSa5Y-like plasmid; strains SA7G and E7G contain an identical plasmid with a replication initiation protein (Rep) based origin. Strains SA7G and E7G additionally contain large plasmids pSA7G1, pSA7G2 and pE7G of ~ 80kb that are not resolved on the gels[79]. **c,** Copy number of pSa5Y in exponentially growing and stationary cells, as determined by quantitative PCR. Bar charts show mean ± sd from three independent experiments (individual dots). **d,** Schematic comparing the pB1067 minimal origin region (dashed lines) with the homologous region of pSa5Y. Sequences encoding equivalents of the experimentally verified RNA I and RNA II from pB1067 are indicated by arrows along with a predicted transcriptional terminator (inverted triangles). **e,** Clustal Omega alignment comparing the pB1067 minimal origin region and the pSa5Y origin region. **f,** Validation of the pSa5Y origin of replication (*ori*). The putative pSa5Y *ori* and *ori* sequences from plasmids pB1067 (pB1067 *ori*), pBAD

(ColE1 *ori*) and pACYC177 (p15A *ori*) were cloned into a conditionally replicating plasmid (pMJ174) containing the *pir*-dependent R6K *ori*. The resulting plasmids were introduced into *pir*- and *pir+ E. coli* strains and spotted on LB+Kan plates. For gel source data, see Supplementary Figure 1.

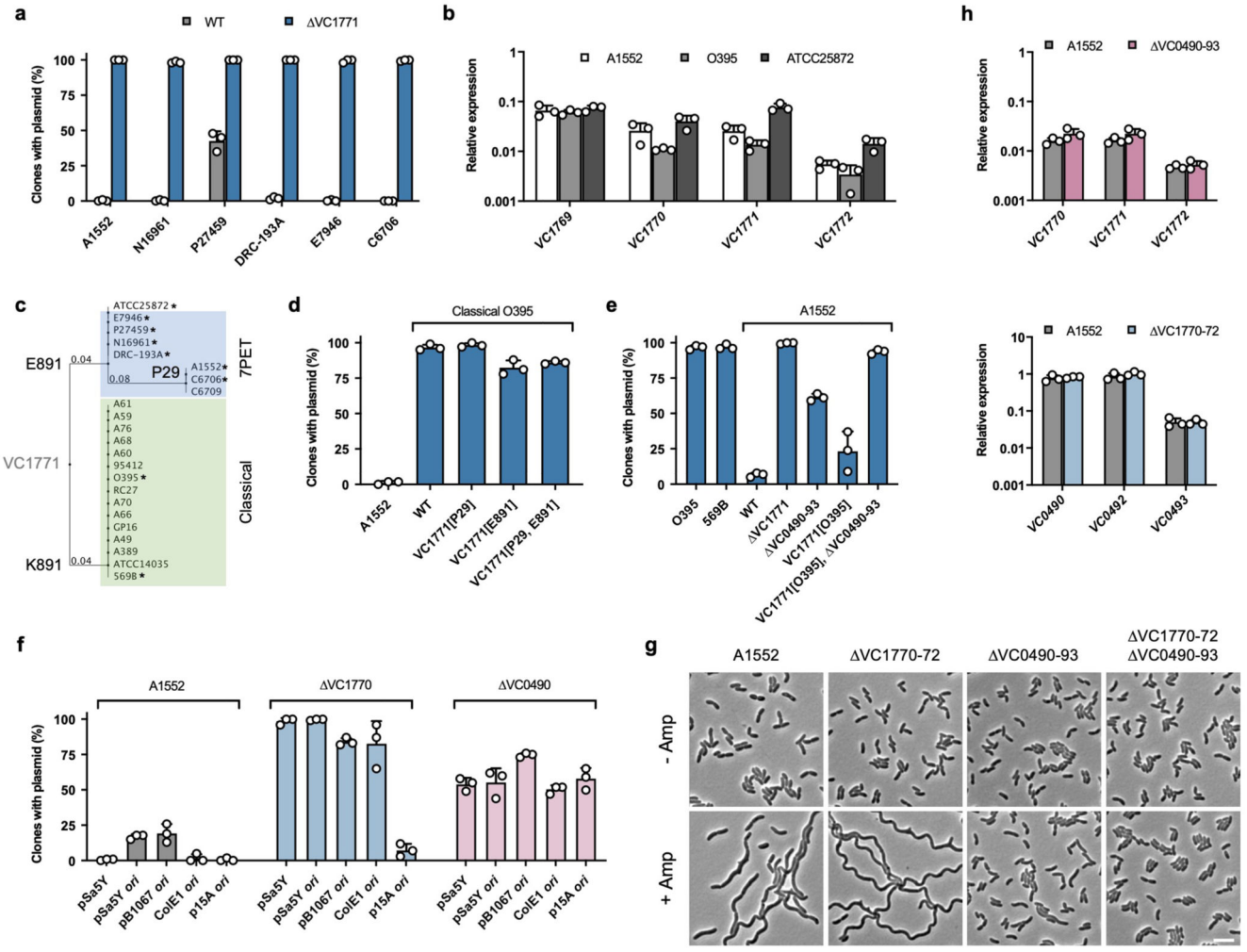

Extended Data Fig. 2. Conservation of the plasmid stability phenotype dependent on VC1771-70 and VC0492-90.

a, pSa5Y-Kan stability in representative wild-type (WT) 7PET strains and their ΔVC1771 derivatives after growth for approx. 50 generations without antibiotic selection. **b,** Comparison of VC1769-1772 transcript levels between strains A1552, classical O395 and ATCC25872 in exponentially growing cells as determined by qRT-PCR. **c,** Phylogenetic tree based on the protein sequence of VC1771 showing that all classical strains examined (green) encode the defective VC1771[K891] variant, whereas all 7PET strains examined (blue) encode the active VC1771[E891] variant. One lineage of 7PET strains encodes an additional S29P substitution. Strains tested in this work are highlighted (*). **d,** Effect of different VC1771 variants on pSa5Y-Amp stability in the classical strain O395. **e,** pSa5Y-Amp stability in strain A1552 encoding a classical variant of VC1771, in the presence and

Europe PMC Funders Author Manuscripts

absence of VC0490-93. **f,** Retention of plasmids with various origins of replication in strain A1552 and its ΔVC1770 and ΔVC0490 derivatives. The different origins of replication (see Methods) were cloned into a neutral plasmid backbone containing a conditional origin of replication inactive in the tested strains. Plasmid stability in (**d-f**) was evaluated after growth for approx. 50 generations without antibiotic selection. **g,** Morphology of exponentially growing cells carrying pBAD, grown in the absence and presence of ampicillin (100 μg/mL), in strain A1552 and its ΔVC1770-72, ΔVC0490-93 and ΔVC1770-72 ΔVC0490-93 derivatives. Images are representative of the results of three independent experiments. Scale bar = 5 μm. **h,** Comparison of transcript levels of VC1770-72 in A1552 and ΔVC0490-93 (top) and VC0490-93 in A1552 and ΔVC1770-72 (bottom) in exponentially growing cells as determined by qRT-PCR. Bar charts show mean ± sd from three independent experiments (individual dots).

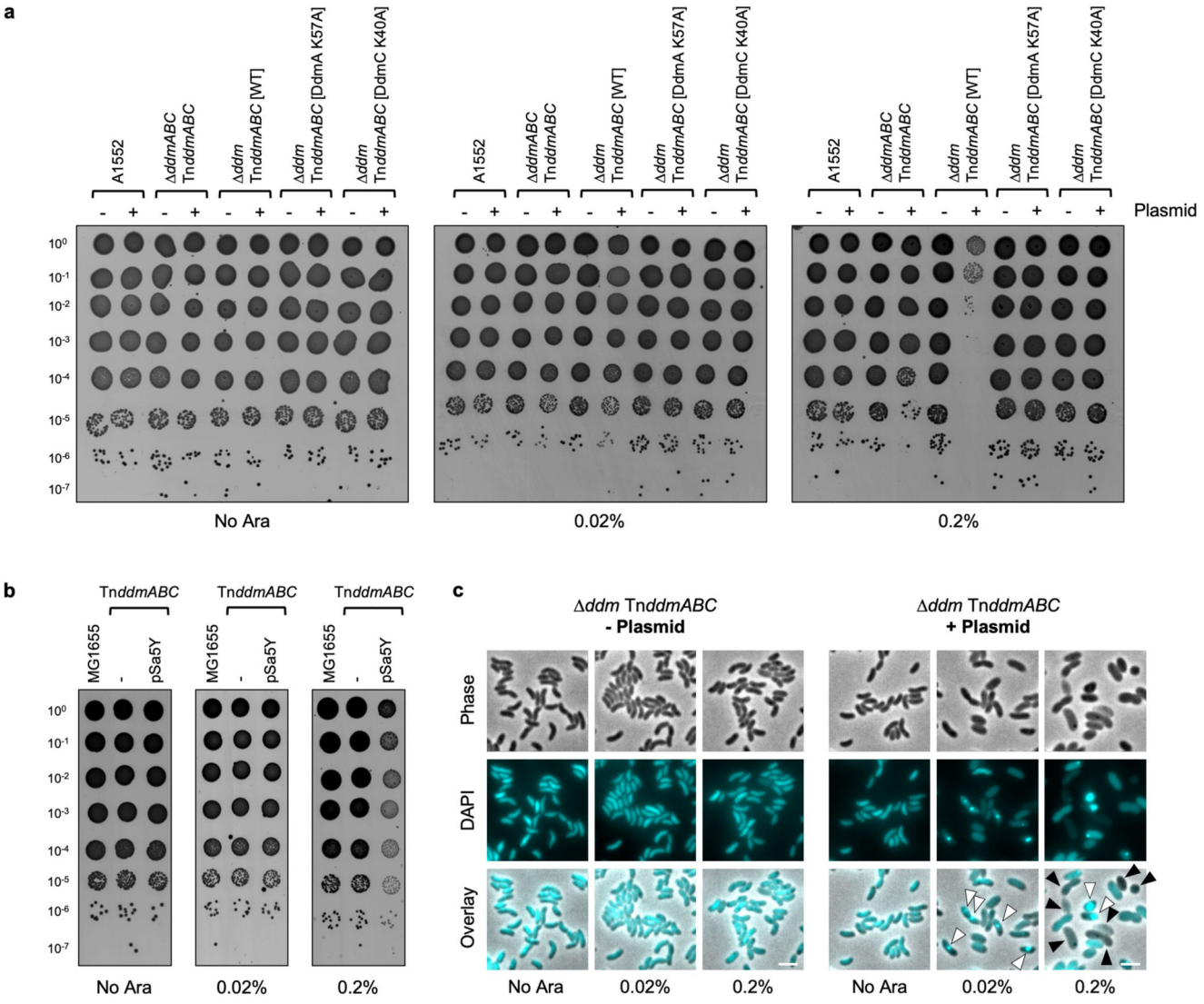

Extended Data Fig. 3. Production of DdmABC leads to plasmid-dependent toxicity in *V. cholerae* and *E. coli*

Europe PMC Funders Author Manuscripts

a, Growth of *V. cholerae* A1552 derivatives carrying arabinose-inducible *ddmABC* (Tn*ddmABC*) or Tn*ddmABC* encoding DdmA and DdmC variants was evaluated on plates, either without additions or supplemented with 0.02% or 0.2% arabinose, in the absence and presence of plasmid pSa5Y-Amp, as indicated. **b,** Growth of *E. coli* MG1655 derivatives carrying *TnddmABC* was evaluated on plates in the absence and presence of plasmid pSa5Y-Kan as in (**a**). Note the transition in appearance of MG1655-Tn*ddmABC* carrying pSa5Y + 0.2% arabinose, switching from dark to pale colonies. **c,** Cells of *V. cholerae* strain Δ*ddm* (Δ*ddmDE* Δ*ddmABC*) *TnddmABC* were imaged following growth for approx. 10 generations in either the absence or presence of 0.02 or 0.2% arabinose, and the absence and presence of pSa5Y-Amp, as indicated. DNA was stained with DAPI. Anucleate cells are indicated with black arrowheads; cells with abnormal nucleoids are indicated with white arrowheads. All images are representative of the results of three independent experiments. Scale bars = 2.5 μm.

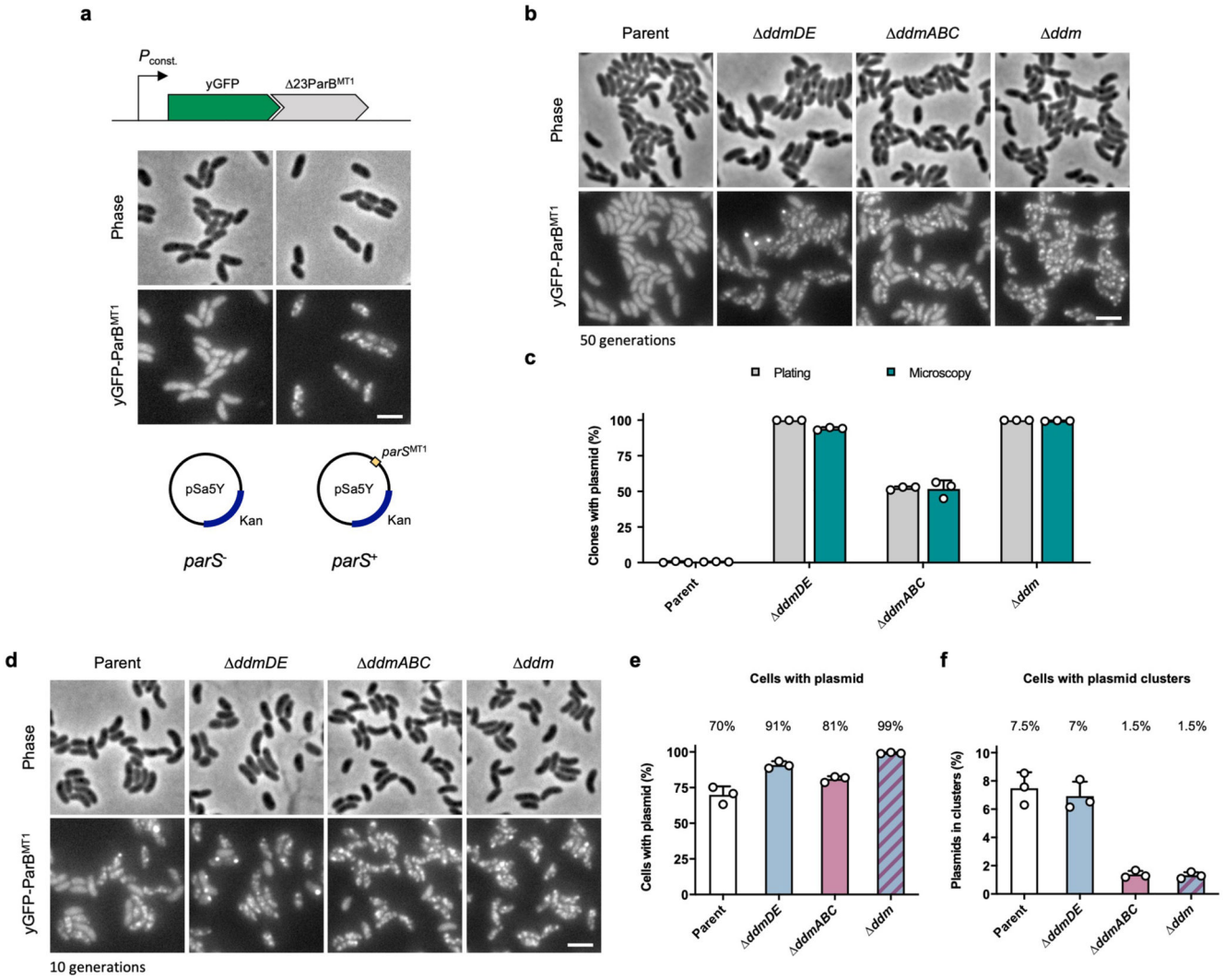

Extended Data Fig. 4. Validation of plasmid stability by *ParB/parS* labelling in individual cells.

a, Visualisation of plasmid pSa5Y in a strain constitutively expressing yGFP-ParB^{MT1} by incorporating the MT1 *parS* site into the plasmid (*parS+*). **b,** pSa5Y-*parS*^{MT1} retention and localisation in single cells of the indicated strains following growth for approx. 50 generations without antibiotic selection. **c,** Comparison of pSa5Y-*parS*^{MT1} stability for the same cultures as in (**b**) determined using either a plating assay or by quantifying the fraction of plasmid-containing cells by microscopy. **d,** pSa5Y-*parS*^{MT1} localisation in single cells of the indicated strains following growth for approx. 10 generations without antibiotic selection. **e-f**, Quantification of the fraction of plasmid containing cells (**e**) and the fraction of cells containing plasmid clusters (**f**) for the cultures shown in (**d**), mean values are shown above the bars. Bar charts show mean ± sd from three independent experiments (individual dots). All strains carry a chromosomally integrated yGFP-ParB^{MT1} fusion. All images are representative of the results of three independent experiments. Scale bars = 2.5 μm.

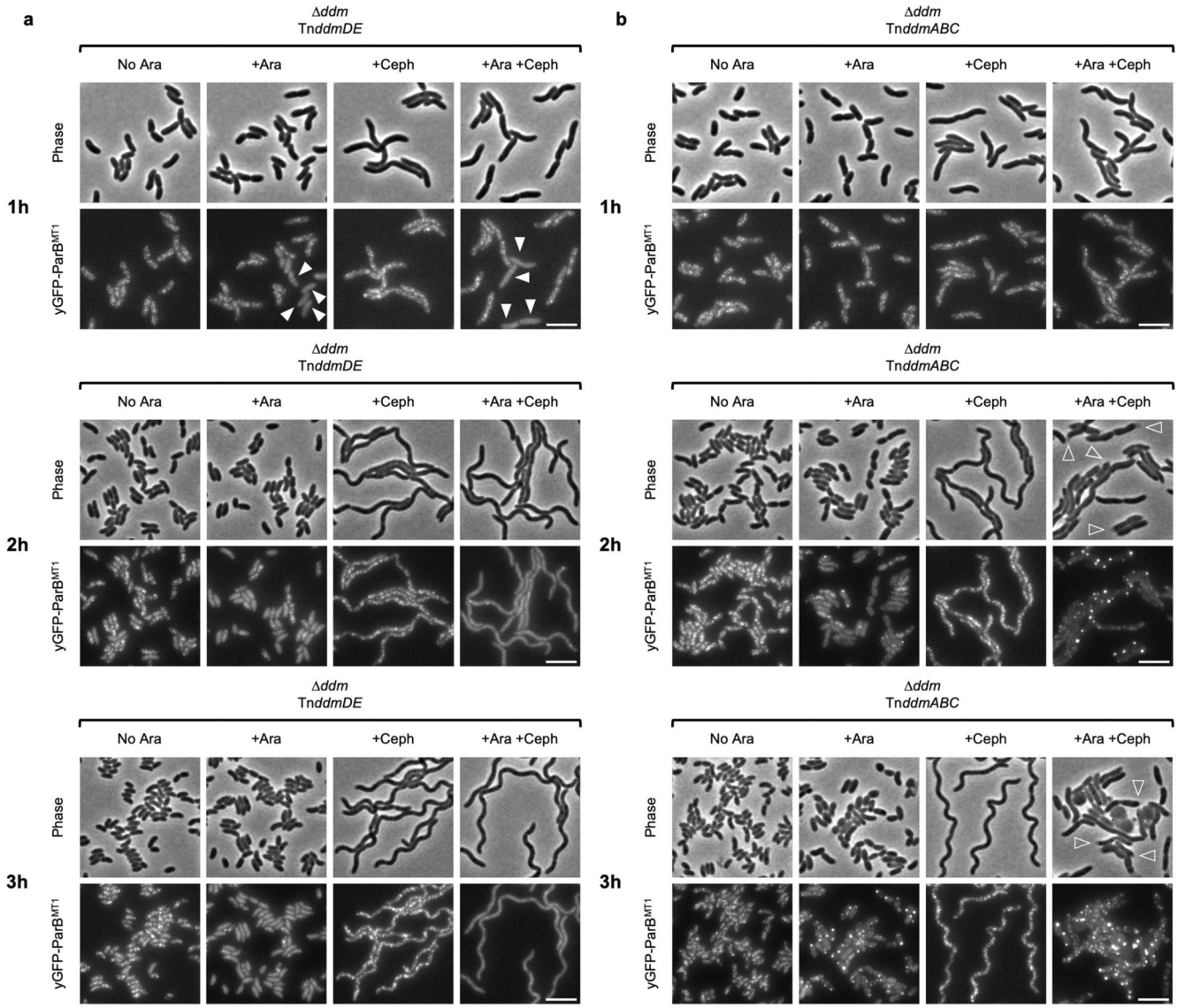

Extended Data Fig. 5. Plasmid elimination by DdmDE is rapid and does not depend on cell division while cell division inhibition enhances plasmid-dependent toxicity by DdmABC.

Time-course showing the effect of DdmDE (**a**) and DdmABC (**b**) production on pSa5Y-*parS*^{MT1} plasmid retention and localisation after addition of cephalexin (Ceph, 5 μg/ml) to block cell division. Arabinose (+Ara) and/or Cephalexin (+Ceph) were added to exponentially growing cells of Δ*ddm* (Δ*ddmDE ΔddmABC*) and imaged after 1, 2 and 3 hours of growth, as indicated. Expression from *TnddmDE* and *TnddmABC* was induced with 0.2 or 0.02% arabinose, respectively. Arrowheads in panel (**a**) highlight examples of plasmid-free cells already detectable after only 1h of *TnddmDE* induction. Open arrowheads in panel (**b**) indicate examples of cells undergoing plasmolysis due to enhanced DdmABC toxicity. All strains carry a chromosomally integrated yGFP-ParB^{MT1} fusion. All images are representative of the results of three independent experiments. Scale bars = 5 μm.

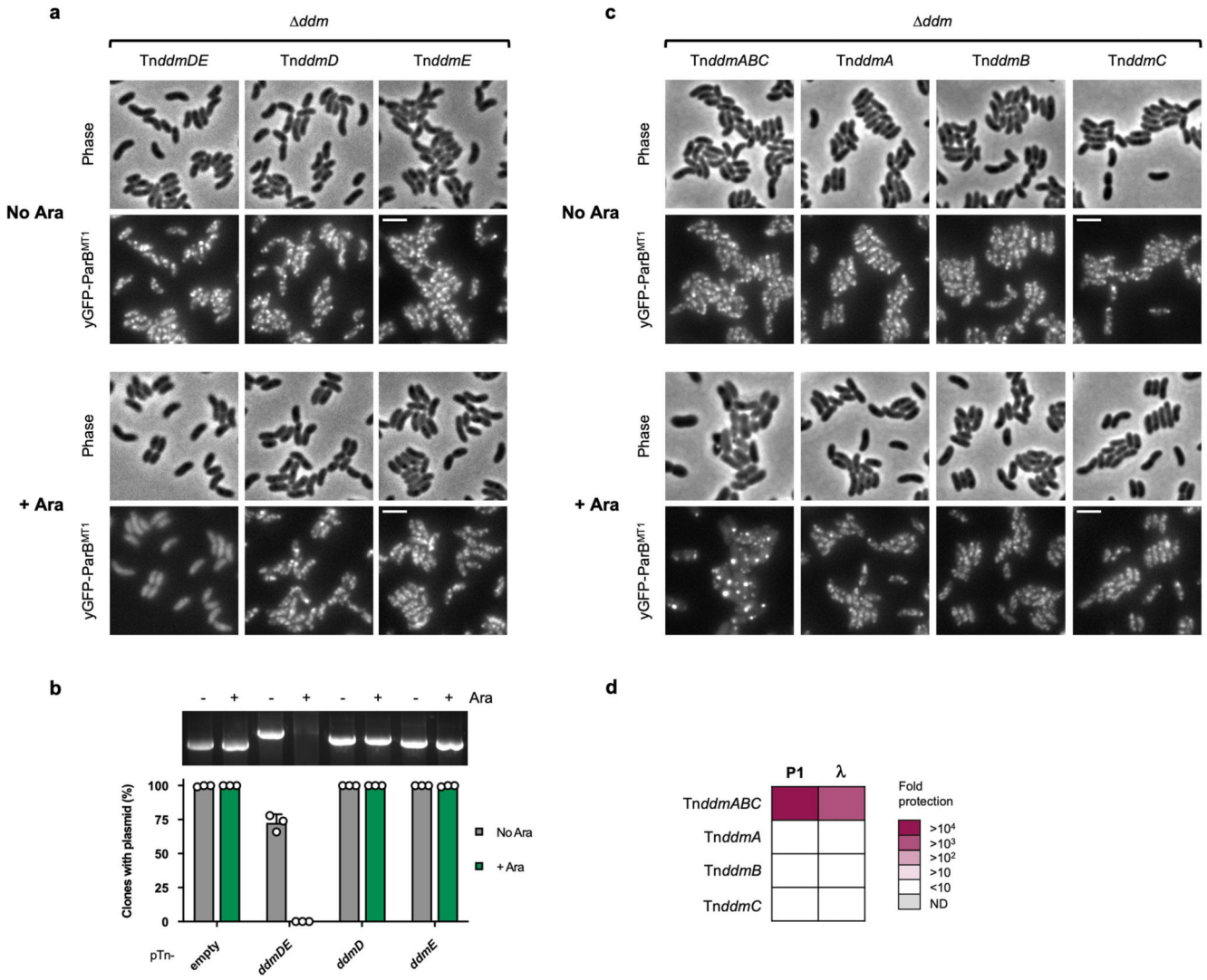

Extended Data Fig. 6. Individual production of DdmD and DdmE or DdmA, DdmB and DdmC does not lead to plasmid and phage-related phenotypes.

a, Effect of individual production of DdmD or DdmE on pSa5Y-*parS*^{MT1} plasmid retention in *V. cholerae ΔddmDE ΔddmABC*). Cells were imaged after growth for approx. 10 generations without antibiotic selection, in the absence (No Ara) and presence (+ Ara) of 0.2% arabinose. **b,** Stability of a conditionally replicating plasmid carrying either an empty transposon or a transposon with inducible *ddmDE*, *ddmD* or *ddmE* in *E. coli* strain S17-1λ*pir*. Cultures were evaluated after growth for approx. 10 generations without antibiotic selection, in the absence (grey bars) and presence (green bars) of 0.2% arabinose. Bar charts show mean ± sd from three independent experiments (individual dots). The inset shows the plasmid extraction yield from the same cultures. For gel source data, see Supplementary Figure 1. **c,** Effect of individual production of DdmA, DdmB or DdmC on pSa5Y-*parS*^{MT1} plasmid localisation in *V. cholerae ΔddmDE ΔddmABC*). Cells were imaged after growth for approx. 10 generations without antibiotic selection, in the absence (No Ara) and presence (+ Ara) of 0.02% arabinose. **d,** Fold protection against coliphages P1 and λ in *E. coli* strain MG1655 conferred by either DdmABC or by DdmA, DdmB and DdmC produced individually. Transposon constructs Tn*ddmABC*, Tn*ddmA*, *TnddmB* and *TnddmC* were integrated in the chromosome and their expression induced by inclusion of 0.2% arabinose in the medium. Fold protection was determined by plaque assays. Strains in panels (**a**) and (**c**) carry a chromosomally integrated yGFP-ParB^{MT1} fusion. All images are representative of the results of three independent experiments. Scale bars = 2.5 μm.

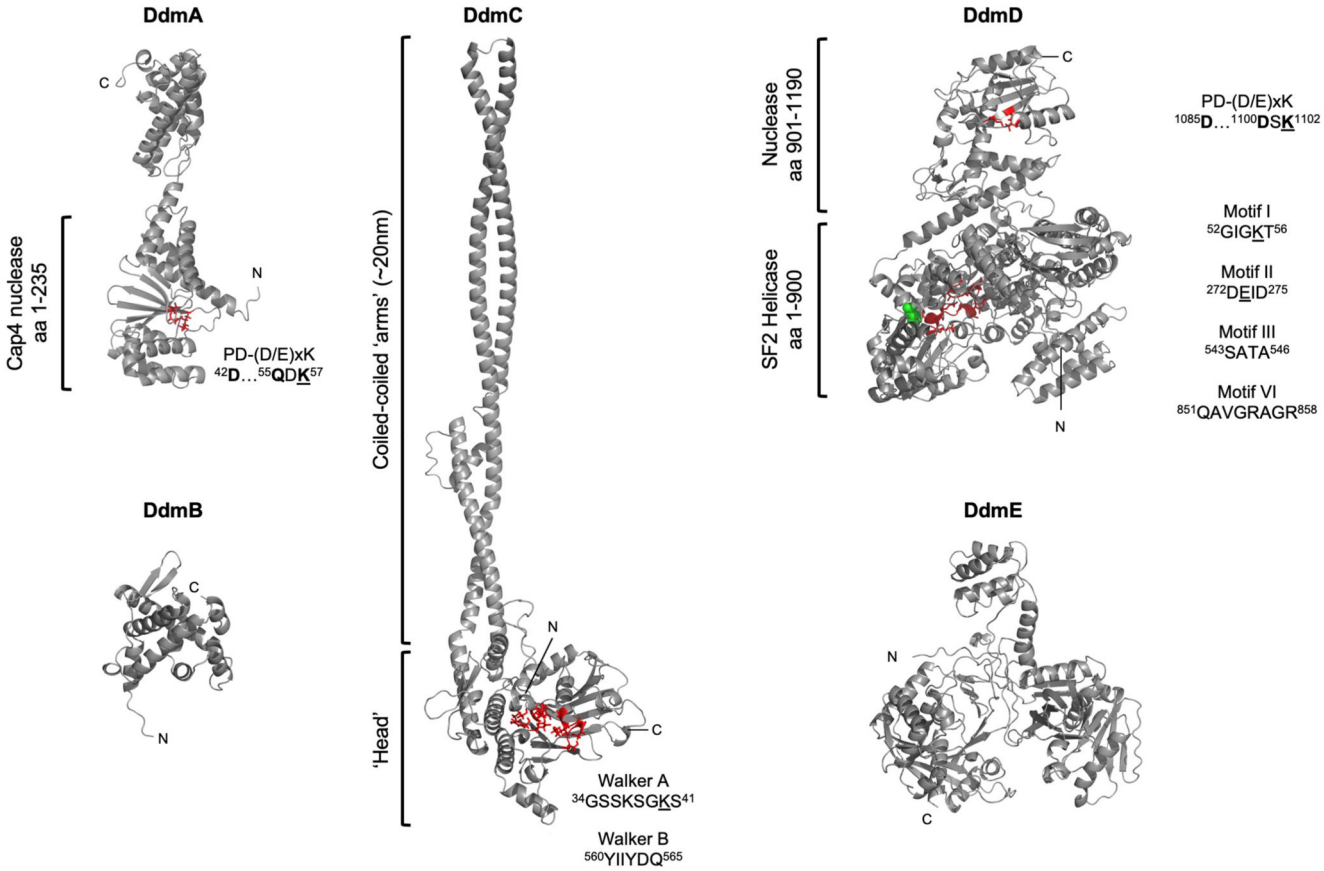

Europe PMC Funders Author Manuscripts

Extended Data Fig. 7. Structural modelling of DdmABC and DdmDE.

Cartoon representations showing the predicted structures of *V. cholerae* strain A1552 DdmABC and DdmDE, highlighting identified functional domains. Side chains of residues predicted to be involved in either nuclease activity or nucleotide binding and hydrolysis are shown as red sticks: DdmA, active site residues of the PD-(D/E)×K superfamily nuclease motif (^{42}**D**...^{55}QDK^{57}); DdmC, the predicted ATP-binding site formed by the N-terminal Walker A motif (^{34}GSSKSGKS^{41}) and the abnormal C-terminal Walker B motif (^{560}YIIYDQ^{565}) and DdmD, superfamily II helicase motifs I (^{52}GIGKT^{56}), II (^{272}DEID^{275}), III (^{543}SATA^{546}) and VI (^{851}QAVGRAGR^{858}) that comprise the predicted ATP-binding site, and active site residues of the PD-(D/E)×K superfamily nuclease motif (^{1085}**D**...^{1100}**DSK**^{1102}). Active site residues of the PD-(D/E)×K motif are shown in bold. Residues targeted by site-directed mutagenesis are underlined. The position of the DdmD residue E891, which in 6th pandemic classical *V. cholerae* strains is typically K891, is shown as a green sphere, located adjacent to the arginine finger (Motif VI). Structural modelling was done using RoseTTAFold (DdmABC) and AlphaFold2 (DdmDE). Images were prepared using PYMOL.

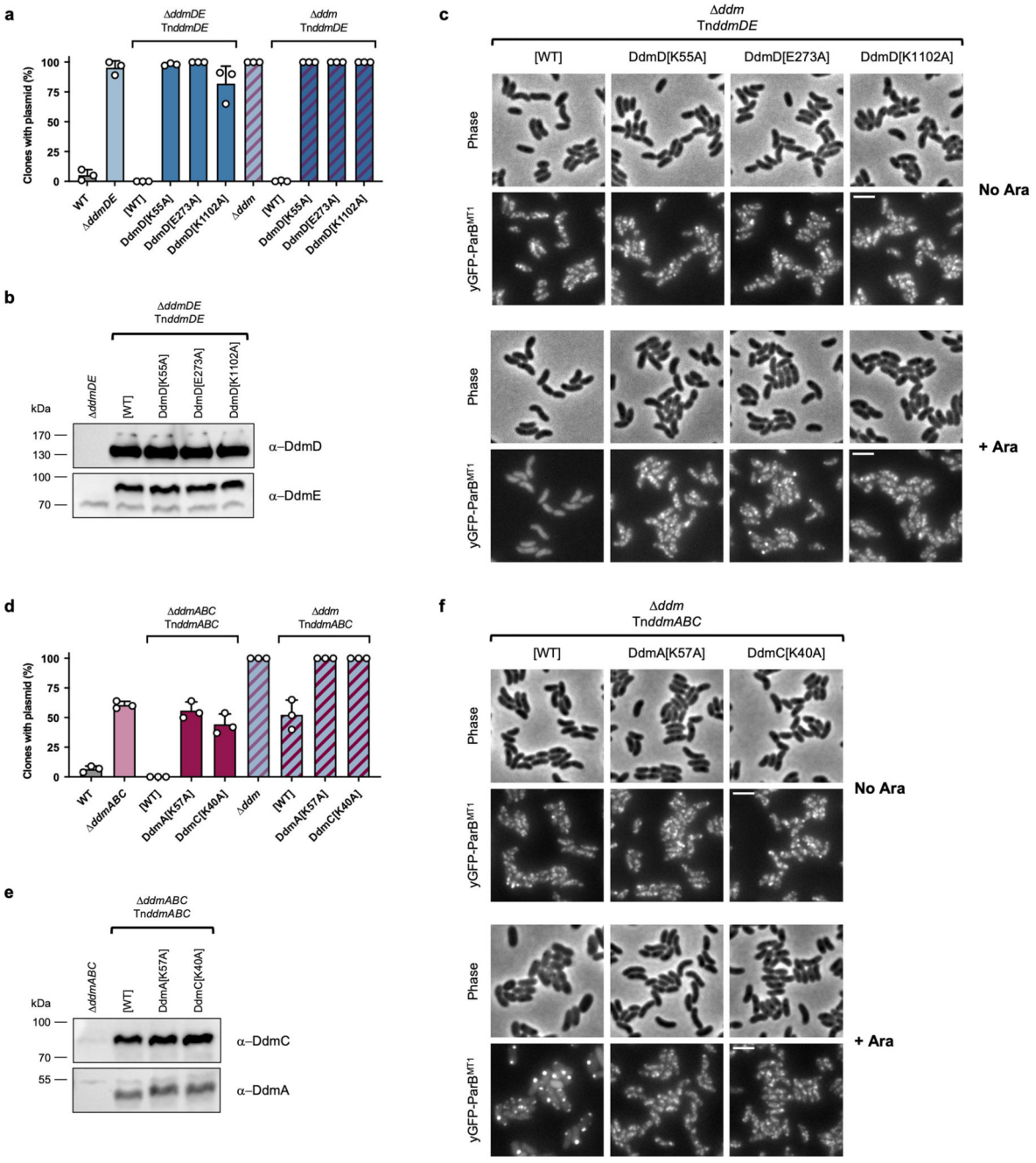

Extended Data Fig. 8. DdmD, DdmA and DdmC variants remain non-functional even when overproduced.

a, pSa5Y-Amp plasmid retention in strains producing DdmD variants from Tn*ddmDE* in a Δ*ddmDE* or Δ*ddm* (Δ*ddmDE* Δ*ddmABC*) background, as indicated, after growth for approx. 50 generations without antibiotic selection. **b,** Western blots showing protein levels of DdmD variants and DdmE. The predicted molecular masses of DdmD and DdmE are 136 and 79.1 kDa, respectively. DdmDE production in (**a**-**b**) was induced by 0.2% arabinose. **c,** Effect of DdmD variants production on pSa5Y-*parS*^{MT1} plasmid retention in a Δ*ddm*

Europe PMC Funders Author Manuscripts

background after growth for approx. 10 generations without antibiotic selection, in the absence (No Ara) and presence of 0.2% arabinose (+ Ara). **d,** pSa5Y-Amp plasmid retention in strains producing DdmA and DdmC variants from *TnddmABC* in a Δ*ddmABC* or Δ*ddm* (Δ*ddmDE* Δ*ddmABC*) background, as indicated, after growth for approx. 50 generations without antibiotic selection. **e,** Western blots showing protein levels of DdmA and DdmC variants. The predicted molecular masses of DdmA and DdmC are 44.5 and 74.6 kDa, respectively. DdmABC production in (**d-e**) was induced by 0.02% arabinose. **f,** Effect of DdmA and DdmC variants production on pSa5Y-*parS*^{MT1} plasmid localisation in a Δ*ddm* background after growth for approx. 10 generations without antibiotic selection, in the absence (No Ara) and presence of 0.02% arabinose (+ Ara). Bar charts show mean ± sd from three independent experiments (individual dots). Strains in panels (**c**) and (**f**) carry a chromosomally integrated yGFP-ParB^{MT1} fusion. All images are representative of the results of three independent experiments. Scale bars = 2.5 μm. For Western blotting source data, see Supplementary Figure 1.

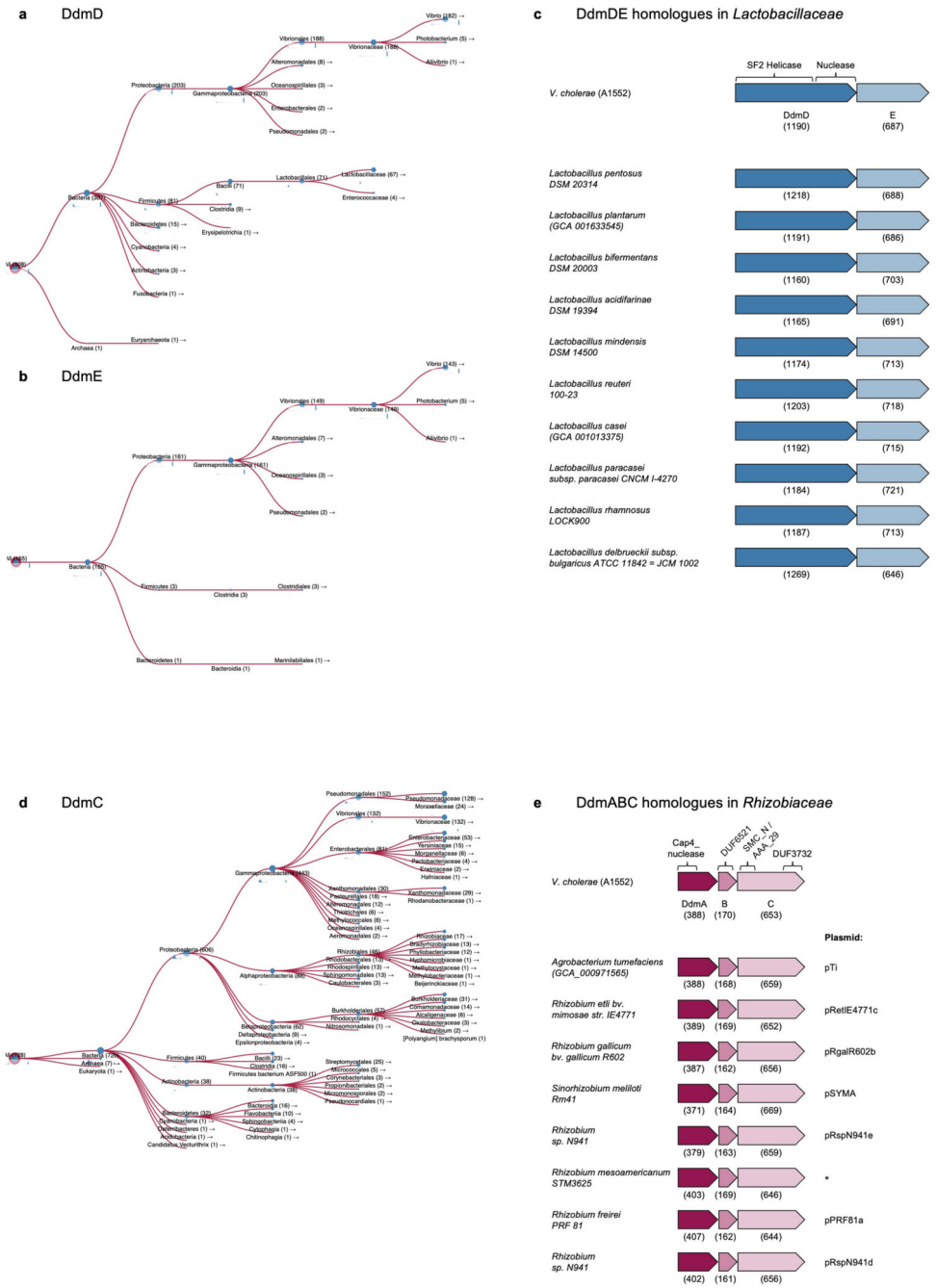

Extended Data Fig. 9. Distribution of DdmDE and DdmABC homologues.

a-b, Taxonomic distribution of putative homologues of DdmD (**a**) and DdmE (**b**) derived from homology searching using PHMMER. The numbers in parentheses at each node indicate the relative number of search hits, and the blue bars represent the distribution of significant hits, respectively, within each taxonomic group. A full list of significant matches is provided in Supplementary Table 2. **c**, Schematics showing examples of intact two-gene *ddmDE* operons within the *Lactobacillaceae*. Operons were identified by examining the genomic loci of PHMMER hits to DdmD within each taxonomic group.

Europe PMC Funders Author Manuscripts

The numbers in parentheses below each gene represent the size of the encoded protein (aa). **d**, Taxonomic distribution of putative homologues of DdmC derived from homology search using PHMMER, as described in (**a**). 685/728 (94%) of the significant matches to DdmC contain the same C-terminal DUF3732. **e**, Schematics showing examples of intact three-gene *ddmABC* operons caried on plasmids of the *Rhizobiaceae*. The presence of *ddmABC* on a plasmid is based either on the sequence annotation or on the proximity (*) to plasmid-specific genes (*repABC* and *tra*).

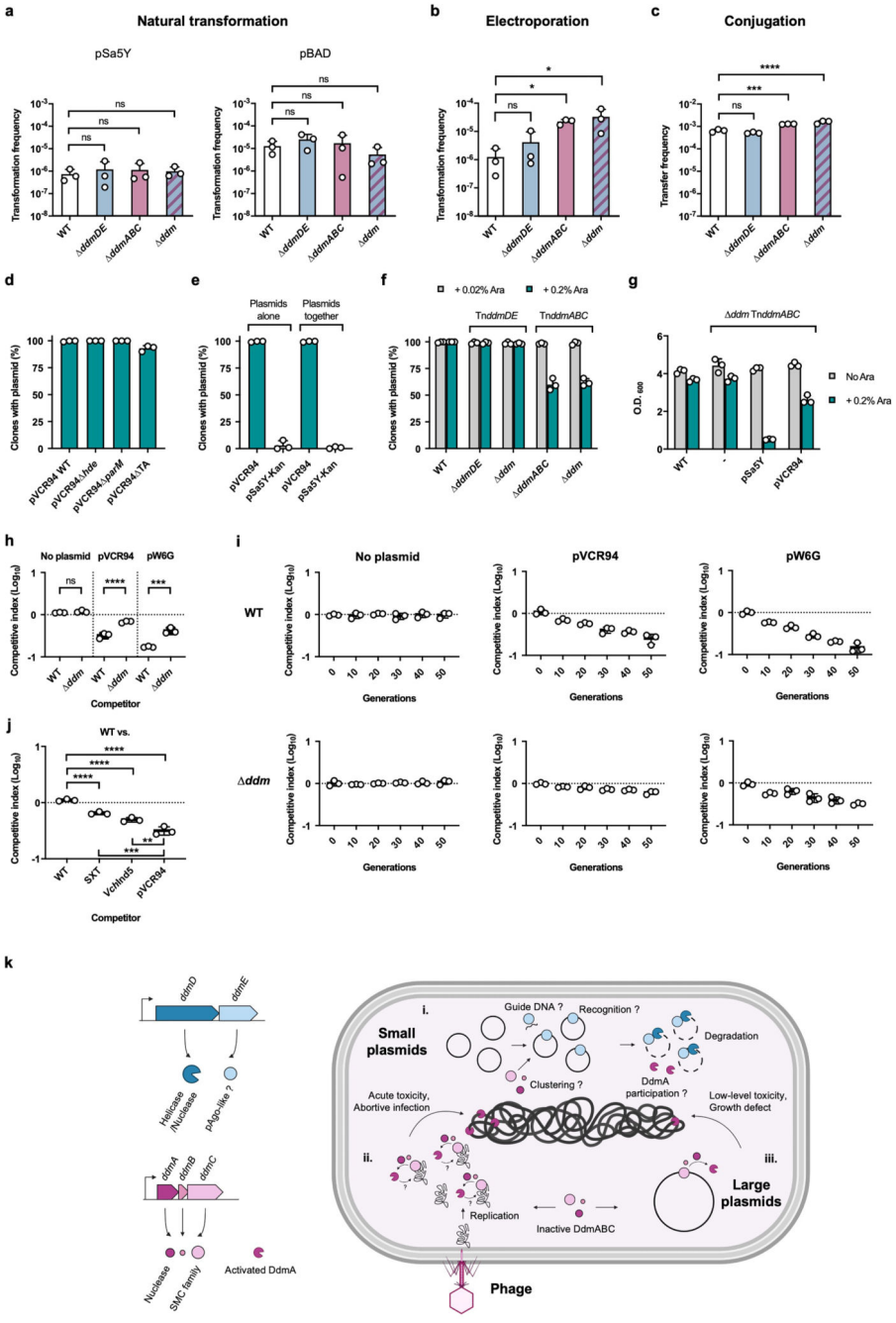

Europe PMC Funders Author Manuscripts

Extended Data Fig. 10. Plasmid acquisition and stability in *V. cholerae* 7PET.

a, Transformation frequencies of indicated strains with plasmid pSa5Y-Kan (left) and pBAD-Kan (right) introduced by natural transformation on chitin. **b,** Transformation frequencies of indicated strains with plasmid pSa5Y-Kan introduced by electroporation. **c,** Conjugative transfer frequencies of indicated strains with plasmid pSa5Y-*oriT*. **d,** Stability of IncC plasmid pVCR94 and its derivatives with deletions in genes encoding the host defence evasion locus (*hde*), a homologue of the partitioning protein ParM, and a toxin-antitoxin system (TA) in strain A1552. **e,** Stability of plasmid pSa5Y-Kan either alone or in a strain carrying plasmid pVCR94. **f,** Stability of plasmid pVCR94 evaluated in the indicated strains, and the expression of *TnddmABC* and *TnddmDE* induced with either 0.02% or 0.2% arabinose, as indicated. Plasmid retention in panels (**d-f**) was evaluated after growth for approx. 50 generations without antibiotic selection. **g,** Effect of DdmABC production on growth evaluated after culturing for 8h in liquid media (equivalent to approx. 10 generations) without antibiotic selection, in the absence and presence of 0.2% arabinose, with either no plasmid, pSa5Y-Amp or pVCR94, as indicated. **h,** Co-culture experiments evaluating competition between A1552 (WT) and Δ*ddm* strains carrying either no plasmid, pVCR94 or pW6G, competed against A1552Δ*lacZ*. **i,** Co-culture experiments evaluating competition over time between A1552Δ*lacZ* and either A1552 (WT) or *A1552*Δ*ddm* (Δ*ddm*), carrying either no plasmid, pVCR94 or pW6G, after growth for approx. 10, 20, 30, 40 and 50 generations without antibiotic selection. **j,** Co-culture experiments evaluating competition between A1552 (WT), A1552-SXT, A1552-*Vch* Ind5 and A1552 carrying pVCR94, competed against A1552Δ*lacZ*. For panels **h** and **j** the competitive index of the indicated strains was evaluated after growth for approx. 50 generations without antibiotic selection. Data represent mean ± sd from three independent experiments (individual dots). Significant differences were determined by one-way ANOVA with either Dunnett's (**a-c**) or Tukey's (**h** and **j**) post-test. *$P < 0.05$; **$P < 0.01$; ***$P < 0.001$; ****$P < 0.0001$; ns – not significant. **k,** Proposed model of elimination of foreign elements by DdmABC and DdmDE. (i) Small multi-copy number plasmids are recognised by DdmE, which in turn leads to plasmid targeting and degradation by the helicase-nuclease DdmD. This process is enhanced by DdmABC, potentially due to its ability to cluster plasmids facilitating recognition by DdmE and/or it may directly participate in plasmid degradation via the nuclease DdmA. (ii-iii) Foreign DNA is recognised by the SMC-like protein DdmC, switching DdmABC to an active state, which in turn leads to activation of DdmA nuclease activity. (ii) Bacteriophage infection and immediate DNA replication leads to strong activation of DdmA, causing acute toxicity via host DNA damage. This results in abortive infection, protecting the population by preventing the release of mature virions. DdmA may also degrade bacteriophage DNA. (iii) Large low copy number plasmids lead to chronic but low-level activation of DdmA, resulting in host DNA damage, that imparts a competitive defect compared to plasmid-free cells. This Abi-like mechanism counter-selects against plasmid carrying cells, leading to their elimination from the population. Created with BioRender.com.

Supplementary Material

Refer to Web version on PubMed Central for supplementary material.

Acknowledgements

We thank Vishwachi Tripathi and Anne-Catherine Portmann for preliminary work on the characterisation of pSa5Y, Sandrine Stutzmann for technical support and, together with Candice Stoudmann, for help with streaking colonies. We further thank Bruno Correia for advice on structural predictions, Stephan Gruber for discussions on SMC-like proteins, Frédérique Le Roux for discussions on MRB-based plasmids, Eduardo Rocha for comments on homologue distribution, and various members of the Blokesch laboratory for valuable discussions. We also wish to acknowledge the kind gifts of strains, plasmids and phages from A. Boehm, V. Burrus, D.K. Chattoraj, A. Dalia, F. Le Roux, J.J. Mekalanos, K.D. Seed, and E.V. Stabb. This work was supported by an ERC Consolidator grant (724630-CholeraIndex) from the European Research Council, and a project grant from the Swiss National Research Foundation (310030_185022) to M.B., and by EPFL intramural funding. M.B. is a Howard Hughes Medical Institute (HHMI) International Research Scholar (Grant #55008726).

Data Availability

The data that support the findings of this study are provided within the manuscript and the associated supplementary materials. Full details and links to the publicly available databases used in bioinformatic analyses are provided in the methods and the associated references. The DNA sequences of newly identified plasmids from environmental *V. cholerae* isolates have been deposited in NCBI's GenBank database with the following accession numbers pSa5Y(CP089143), pSO5Y(CP089144), pSA7G3(CP089145), pSL4G(CP089146), and pE7G2(CP089147).

References

1. Bernheim A, Sorek R. The pan-immune system of bacteria: antiviral defence as a community resource. Nat Rev Microbiol. 2020; 18: 113–19. DOI: 10.1038/s41579-019-0278-2 [PubMed: 31695182]
2. Clemens JD, Nair GB, Ahmed T, Qadri F, Holmgren J. Cholera. The Lancet. 2017; 390: 1539–49. DOI: 10.1016/S0140-6736(17)30559-7
3. Faruque SM, Albert MJ, Mekalanos JJ. Epidemiology, genetics, and ecology of toxigenic Vibrio cholerae. Microbiol Mol Biol Rev. 1998; 62: 1301–14. [PubMed: 9841673]
4. Chun J, et al. Comparative genomics reveals mechanism for short-term and long-term clonal transitions in pandemic Vibrio cholerae. Proc Natl Acad Sci U S A. 2009; 106: 15442–7. DOI: 10.1073/pnas.0907787106 [PubMed: 19720995]
5. Waldor MK, Mekalanos JJ. Lysogenic conversion by a filamentous phage encoding cholera toxin. Science. 1996; 272: 1910–4. DOI: 10.1126/science.272.5270.1910 [PubMed: 8658163]
6. Karaolis DK, et al. A Vibrio cholerae pathogenicity island associated with epidemic and pandemic strains. Proc Natl Acad Sci U S A. 1998; 95: 3134–9. DOI: 10.1073/pnas.95.6.3134 [PubMed: 9501228]
7. Jermyn WS, Boyd EF. Characterization of a novel Vibrio pathogenicity island (VPI-2) encoding neuraminidase (nanH) among toxigenic Vibrio cholerae isolates. Microbiology. 2002; 148: 3681–93. DOI: 10.1099/00221287-148-11-3681 [PubMed: 12427958]
8. Dziejman M, et al. Comparative genomic analysis of Vibrio cholerae: genes that correlate with cholera endemic and pandemic disease. Proc Natl Acad Sci U S A. 2002; 99: 1556–61. DOI: 10.1073/pnas.042667999 [PubMed: 11818571]
9. O'Shea YA, et al. The Vibrio seventh pandemic island-II is a 26.9 kb genomic island present in Vibrio cholerae El Tor and O139 serogroup isolates that shows homology to a 43.4 kb genomic island in V. vulnificus. Microbiology. 2004; 150: 4053–63. DOI: 10.1099/mic.0.27172-0 [PubMed: 15583158]
10. Hu D, et al. Origins of the current seventh cholera pandemic. Proc Natl Acad Sci U S A. 2016; 113: E7730–E39. DOI: 10.1073/pnas.1608732113 [PubMed: 27849586]

11. Rodríguez-Beltrán J, Dela Fuente J, León-Sampedro R, MacLean RC, San Millan A. Beyond horizontal gene transfer: the role of plasmids in bacterial evolution. Nat Rev Microbiol. 2021; 19: 347–59. DOI: 10.1038/s41579-020-00497-1 [PubMed: 33469168]
12. San Millan A, MacLean RC. Fitness Costs of Plasmids: a Limit to Plasmid Transmission. Microbiol Spectr. 2017; 5 doi: 10.1128/microbiolspec.MTBP-0016-2017
13. Le Roux F, Davis BM, Waldor MK. Conserved small RNAs govern replication and incompatibility of a diverse new plasmid family from marine bacteria. Nucleic Acids Res. 2011; 39: 1004–13. DOI: 10.1093/nar/gkq852 [PubMed: 20923782]
14. Pan L, Leung PC, Gu JD. A new ColE1-like plasmid group revealed by comparative analysis of the replication proficient fragments of Vibrionaceae plasmids. J Microbiol Biotechnol. 2010; 20: 1163–78. DOI: 10.4014/jmb.1003.03007 [PubMed: 20798577]
15. Xue H, et al. Eco-Evolutionary Dynamics of Episomes among Ecologically Cohesive Bacterial Populations. mBio. 2015; 6 e00552-15 doi: 10.1128/mBio.00552-15 [PubMed: 25944863]
16. Rahal K, Gerbaud G, Bouanchaud DH. Stability of R plasmids belonging to different incompatibility groups in Vibrio cholerae "Eltor". Ann Microbiol (Paris). 1978; 129: 409–14. [PubMed: 697261]
17. Newland JW, Voll MJ, McNicol LA. Serology and plasmid carriage in Vibrio cholerae. Canadian Journal of Microbiology. 1984; 30: 1149–56. DOI: 10.1139/m84-180 [PubMed: 6095986]
18. Amaro C, Aznar R, Garay E, Alcaide E. R plasmids in environmental Vibrio cholerae non-O1 strains. Appl Environ Microbiol. 1988; 54: 2771–6. [PubMed: 3214157]
19. Weill FX, et al. Genomic history of the seventh pandemic of cholera in Africa. Science. 2017; 358: 785–89. DOI: 10.1126/science.aad5901 [PubMed: 29123067]
20. Box AM, McGuffie MJ, O'Hara BJ, Seed KD. Functional Analysis of Bacteriophage Immunity through a Type I-E CRISPR-Cas System in Vibrio cholerae and Its Application in Bacteriophage Genome Engineering. J Bacteriol. 2016; 198: 578–90. DOI: 10.1128/JB.00747-15 [PubMed: 26598368]
21. Ryazansky S, Kulbachinskiy A, Aravin AA. The Expanded Universe of Prokaryotic Argonaute Proteins. mBio. 2018; 9 e01935-18 doi: 10.1128/mBio.01935-18 [PubMed: 30563906]
22. Dunn AK, Millikan DS, Adin DM, Bose JL, Stabb EV. New rfp-and pES213-derived tools for analyzing symbiotic Vibrio fischeri reveal patterns of infection and lux expression in situ. Appl Environ Microbiol. 2006; 72: 802–10. DOI: 10.1128/AEM.72.1.802-810.2006 [PubMed: 16391121]
23. Waldor MK, Mekalanos JJ. Emergence of a new cholera pandemic: molecular analysis of virulence determinants in Vibrio cholerae O139 and development of a live vaccine prototype. J Infect Dis. 1994; 170: 278–83. DOI: 10.1093/infdis/170.2.278 [PubMed: 8035010]
24. Blokesch M, Schoolnik GK. Serogroup conversion of Vibrio cholerae in aquatic reservoirs. PLoS Pathog. 2007; 3 e81 doi: 10.1371/journal.ppat.0030081 [PubMed: 17559304]
25. Doron S, et al. Systematic discovery of antiphage defense systems in the microbial pangenome. Science. 2018; 359 eaar4120 doi: 10.1126/science.aar4120 [PubMed: 29371424]
26. Makarova KS, Wolf YI, Snir S, Koonin EV. Defense islands in bacterial and archaeal genomes and prediction of novel defense systems. J Bacteriol. 2011; 193: 6039–56. DOI: 10.1128/JB.05535-11 [PubMed: 21908672]
27. Kuzmenko A, et al. DNA targeting and interference by a bacterial Argonaute nuclease. Nature. 2020; 587: 632–37. DOI: 10.1038/s41586-020-2605-1 [PubMed: 32731256]
28. Lopatina A, Tal N, Sorek R. Abortive Infection: Bacterial Suicide as an Antiviral Immune Strategy. Annu Rev Virol. 2020; 7: 371–84. DOI: 10.1146/annurev-virology-011620-040628 [PubMed: 32559405]
29. Nielsen HJ, Ottesen JR, Youngren B, Austin SJ, Hansen FG. The Escherichia coli chromosome is organized with the left and right chromosome arms in separate cell halves. Mol Microbiol. 2006; 62: 331–8. DOI: 10.1111/j.1365-2958.2006.05346.x [PubMed: 17020576]
30. Fairman-Williams ME, Guenther UP, Jankowsky E. SF1 and SF2 helicases: family matters. Curr Opin Struct Biol. 2010; 20: 313–24. DOI: 10.1016/j.sbi.2010.03.011 [PubMed: 20456941]

31. Steczkiewicz K, Muszewska A, Knizewski L, Rychlewski L, Ginalski K. Sequence, structure and functional diversity of PD-(D/E)XK phosphodiesterase superfamily. Nucleic Acids Res. 2012; 40: 7016–45. DOI: 10.1093/nar/gks382 [PubMed: 22638584]
32. Swarts DC, et al. DNA-guided DNA interference by a prokaryotic Argonaute. Nature. 2014; 507: 258–61. DOI: 10.1038/nature12971 [PubMed: 24531762]
33. Nolivos S, Sherratt D. The bacterial chromosome: architecture and action of bacterial SMC and SMC-like complexes. FEMS Microbiol Rev. 2014; 38: 380–92. DOI: 10.1111/1574-6976.12045 [PubMed: 24118085]
34. Rybenkov VV, Herrera V, Petrushenko ZM, Zhao H. MukBEF, a chromosomal organizer. J Mol Microbiol Biotechnol. 2014; 24: 371–83. DOI: 10.1159/000369099 [PubMed: 25732339]
35. Pellegrino S, et al. Structural and functional characterization of an SMC-like protein RecN: new insights into double-strand break repair. Structure. 2012; 20: 2076–89. DOI: 10.1016/j.str.2012.09.010 [PubMed: 23085075]
36. Petrushenko ZM, She W, Rybenkov VV. A new family of bacterial condensins. Mol Microbiol. 2011; 81: 881–96. DOI: 10.1111/j.1365-2958.2011.07763.x [PubMed: 21752107]
37. Panas MW, et al. Noncanonical SMC protein in Mycobacterium smegmatis restricts maintenance of Mycobacterium fortuitum plasmids. Proc Natl Acad Sci U S A. 2014; 111: 13264–71. DOI: 10.1073/pnas.1414207111 [PubMed: 25197070]
38. Lowey B, et al. CBASS Immunity Uses CARF-Related Effectors to Sense 3'-5'-and 2'-5'-Linked Cyclic Oligonucleotide Signals and Protect Bacteria from Phage Infection. Cell. 2020; 182: 38–49. e17 doi: 10.1016/j.cell.2020.05.019 [PubMed: 32544385]
39. Krishnan A, Burroughs AM, Iyer LM, Aravind L. Comprehensive classification of ABC ATPases and their functional radiation in nucleoprotein dynamics and biological conflict systems. Nucleic Acids Res. 2020; 48: 10045–75. DOI: 10.1093/nar/gkaa726 [PubMed: 32894288]
40. Carraro N, et al. Development of pVCR94DeltaX from Vibrio cholerae, a prototype for studying multidrug resistant IncA/C conjugative plasmids. Front Microbiol. 2014; 5: 44. doi: 10.3389/fmicb.2014.00044 [PubMed: 24567731]
41. Harmer CJ, Hall RM. The A to Z of A/C plasmids. Plasmid. 2015; 80: 63–82. DOI: 10.1016/j.plasmid.2015.04.003 [PubMed: 25910948]
42. Hancock SJ, et al. Identification of IncA/C Plasmid Replication and Maintenance Genes and Development of a Plasmid Multilocus Sequence Typing Scheme. Antimicrob Agents Chemother. 2017; 61 e01740-16 doi: 10.1128/AAC.01740-16 [PubMed: 27872077]
43. Roy D, Huguet KT, Grenier F, Burrus V. IncC conjugative plasmids and SXT/R391 elements repair double-strand breaks caused by CRISPR–Cas during conjugation. Nucleic Acids Res. 2020; 48: 8815–27. DOI: 10.1093/nar/gkaa518 [PubMed: 32556263]
44. Wozniak RA, et al. Comparative ICE genomics: insights into the evolution of the SXT/R391 family of ICEs. PLoS Genet. 2009; 5 e1000786 doi: 10.1371/journal.pgen.1000786 [PubMed: 20041216]
45. Cohen D, et al. Cyclic GMP-AMP signalling protects bacteria against viral infection. Nature. 2019; 574: 691–95. DOI: 10.1038/s41586-019-1605-5 [PubMed: 31533127]
46. Decorsière A, et al. Hepatitis B virus X protein identifies the Smc5/6 complex as a host restriction factor. Nature. 2016; 531: 386–89. DOI: 10.1038/nature17170 [PubMed: 26983541]
47. Lopatkin AJ, et al. Persistence and reversal of plasmid-mediated antibiotic resistance. Nat Commun. 2017; 8: 1689. doi: 10.1038/s41467-017-01532-1 [PubMed: 29162798]
48. LeGault KN, et al. Temporal shifts in antibiotic resistance elements govern phage-pathogen conflicts. Science. 2021; 373 eabg2166 doi: 10.1126/science.abg2166 [PubMed: 34326207]
49. Berryhill BA, Garcia R, Manuel JA, Levin BR. The ecological consequences and evolution of retron-mediated suicide as a way to protect Escherichia coli from being killed by phage. bioRxiv. 2021; doi: 10.1101/2021.05.05.442803
50. Davies BW, Bogard RW, Young TS, Mekalanos JJ. Coordinated regulation of accessory genetic elements produces cyclic di-nucleotides for V. cholerae virulence. Cell. 2012; 149: 358–70. DOI: 10.1016/j.cell.2012.01.053 [PubMed: 22500802]
51. Severin GB, et al. Direct activation of a phospholipase by cyclic GMP-AMP in El Tor Vibrio cholerae. Proc Natl Acad Sci U S A. 2018; 115: E6048–E55. DOI: 10.1073/pnas.1801233115 [PubMed: 29891656]

52. Severin GB, et al. A Broadly Conserved Deoxycytidine Deaminase Protects Bacteria from Phage Infection. bioRxiv. 2021; doi: 10.1101/2021.03.31.437871
53. Taviani E, et al. Discovery of novel Vibrio cholerae VSP-II genomic islands using comparative genomic analysis. FEMS Microbiol Lett. 2010; 308: 130–7. DOI: 10.1111/j.1574-6968.2010.02008.x [PubMed: 20528940]
54. Matthey N, Drebes Dörr NC, Blokesch M. Long-Read-Based Genome Sequences of Pandemic and Environmental Vibrio cholerae Strains. Microbiol Resour Announc. 2018; 7 e01574-18 doi: 10.1128/MRA.01574-18 [PubMed: 30574591]
55. Marvig RL, Blokesch M. Natural transformation of Vibrio cholerae as a tool--optimizing the procedure. BMC Microbiol. 2010; 10: 155. doi: 10.1186/1471-2180-10-155 [PubMed: 20509862]
56. Meibom KL, Blokesch M, Dolganov NA, Wu CY, Schoolnik GK. Chitin induces natural competence in Vibrio cholerae. Science. 2005; 310: 1824–7. DOI: 10.1126/science.1120096 [PubMed: 16357262]
57. Sambrook, J, Fritsch, EF, Maniatis, T. Molecular Cloning: A Laboratory Manual. Cold Spring Harbor Laboratory Press; Cold Spring Harbor: 1989.
58. De Souza Silva O, Blokesch M. Genetic manipulation of Vibrio cholerae by combining natural transformation with FLP recombination. Plasmid. 2010; 64: 186–95. DOI: 10.1016/j.plasmid.2010.08.001 [PubMed: 20709100]
59. Blokesch M. TransFLP--a method to genetically modify Vibrio cholerae based on natural transformation and FLP-recombination. J Vis Exp. 2012; 68 e3761 doi: 10.3791/3761
60. Meibom KL, et al. The Vibrio cholerae chitin utilization program. Proc Natl Acad Sci U S A. 2004; 101: 2524–9. DOI: 10.1073/pnas.0308707101 [PubMed: 14983042]
61. Bao Y, Lies DP, Fu H, Roberts GP. An improved Tn7-based system for the single-copy insertion of cloned genes into chromosomes of gram-negative bacteria. Gene. 1991; 109: 167–68. DOI: 10.1016/0378-1119(91)90604-A [PubMed: 1661697]
62. Keymer DP, Miller MC, Schoolnik GK, Boehm AB. Genomic and phenotypic diversity of coastal Vibrio cholerae strains is linked to environmental factors. Appl Environ Microbiol. 2007; 73: 3705–14. DOI: 10.1128/AEM.02736-06 [PubMed: 17449702]
63. Gurung I, Berry JL, Hall AMJ, Pelicic V. Cloning-independent markerless gene editing in Streptococcus sanguinis: novel insights in type IV pilus biology. Nucleic Acids Res. 2017; 45 e40 doi: 10.1093/nar/gkw1177 [PubMed: 27903891]
64. Van der Henst C, et al. Molecular insights into Vibrio cholerae's intra-amoebal host-pathogen interactions. Nat Commun. 2018; 9: 3460. doi: 10.1038/s41467-018-05976-x [PubMed: 30150745]
65. Lee C, Kim J, Shin SG, Hwang S. Absolute and relative QPCR quantification of plasmid copy number in Escherichia coli. J Biotechnol. 2006; 123: 273–80. DOI: 10.1016/j.jbiotec.2005.11.014 [PubMed: 16388869]
66. Lo Scrudato M, Blokesch M. The regulatory network of natural competence and transformation of Vibrio cholerae. PLoS Genet. 2012; 8 e1002778 doi: 10.1371/journal.pgen.1002778 [PubMed: 22737089]
67. Dalia AB, Dalia TN. Spatiotemporal Analysis of DNA Integration during Natural Transformation Reveals a Mode of Nongenetic Inheritance in Bacteria. Cell. 2019; 179: 1499–511. e10 doi: 10.1016/j.cell.2019.11.021 [PubMed: 31835029]
68. Finn RD, Clements J, Eddy SR. HMMER web server: interactive sequence similarity searching. Nucleic Acids Res. 2011; 39: W29–W37. DOI: 10.1093/nar/gkr367 [PubMed: 21593126]
69. Potter SC, et al. HMMER web server: 2018 update. Nucleic Acids Res. 2018; 46: W200–W04. DOI: 10.1093/nar/gky448 [PubMed: 29905871]
70. Söding J, Biegert A, Lupas AN. The HHpred interactive server for protein homology detection and structure prediction. Nucleic Acids Res. 2005; 33: W244–W48. DOI: 10.1093/nar/gki408 [PubMed: 15980461]
71. Zimmermann L, et al. A Completely Reimplemented MPI Bioinformatics Toolkit with a New HHpred Server at its Core. Journal of Molecular Biology. 2018; 430: 2237–43. DOI: 10.1016/j.jmb.2017.12.007 [PubMed: 29258817]

72. Kelley LA, Mezulis S, Yates CM, Wass MN, Sternberg MJE. The Phyre2 web portal for protein modeling, prediction and analysis. Nature Protocols. 2015; 10: 845–58. DOI: 10.1038/nprot.2015.053 [PubMed: 25950237]

73. Yang J, Zhang Y. I-TASSER server: new development for protein structure and function predictions. Nucleic Acids Res. 2015; 43: W174–W81. DOI: 10.1093/nar/gkv342 [PubMed: 25883148]

74. Baek M, et al. Accurate prediction of protein structures and interactions using a three-track neural network. Science. 2021; 373: 871–76. DOI: 10.1126/science.abj8754 [PubMed: 34282049]

75. Mirdita M, Ovchinnikov S, Steinegger M. ColabFold-Making protein folding accessible to all. bioRxiv. 2021; doi: 10.1101/2021.08.15.456425

76. Jumper J, et al. Highly accurate protein structure prediction with AlphaFold. Nature. 2021; 596: 583–89. DOI: 10.1038/s41586-021-03819-2 [PubMed: 34265844]

77. McDonnell AV, Jiang T, Keating AE, Berger B. Paircoil2: improved prediction of coiled coils from sequence. Bioinformatics. 2006; 22: 356–8. DOI: 10.1093/bioinformatics/bti797 [PubMed: 16317077]

78. Li X, et al. oriTfinder: a web-based tool for the identification of origin of transfers in DNA sequences of bacterial mobile genetic elements. Nucleic Acids Res. 2018; 46: W229–W34. DOI: 10.1093/nar/gky352 [PubMed: 29733379]

79. Drebes Dörr NC, Blokesch M. Interbacterial competition and anti-predatory behaviour of environmental Vibrio cholerae strains. Environ Microbiol. 2020; 22: 4485–504. DOI: 10.1111/1462-2920.15224 [PubMed: 32885535]

Europe PMC Funders Author Manuscripts

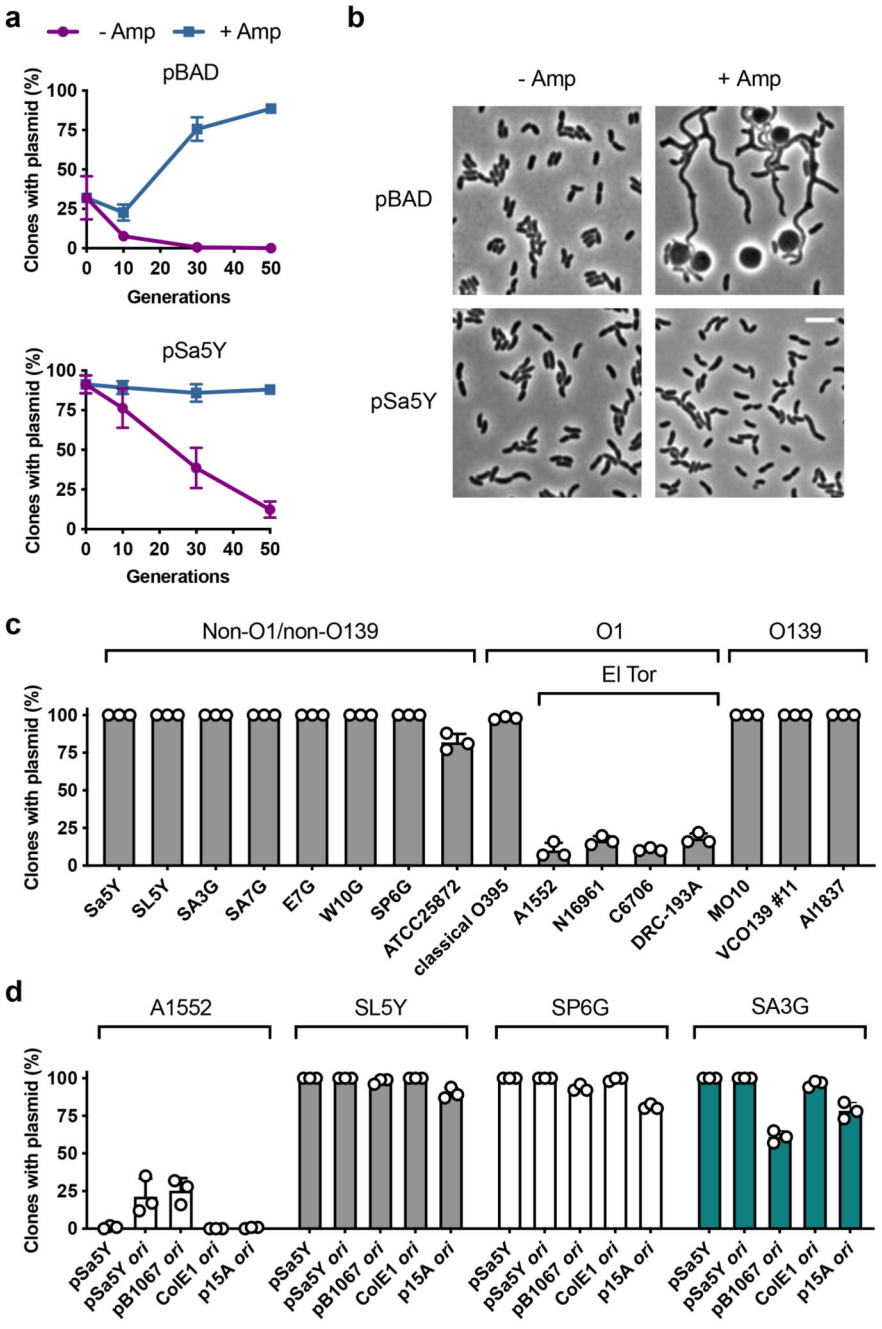

Fig. 1. Plasmids are unstable in *V. cholerae* O1 El Tor.

a, Time-course of pBAD and pSa5Y (pSa5Y-Amp) stability in 7PET strain A1552. Strains were grown without (-Amp) and with (+Amp) selection, with sampling after growth for 0 and approx. 10, 30 and 50 generations. **b,** Morphology of exponentially growing cells carrying either pBAD or pSa5Y without and with ampicillin (100 μg/ml), as indicated. Images are representative of three independent experiments. Scale bar = 5 μm. **c,** Retention of pSa5Y (pSa5Y-Kan) in various O1, O139 and non-O1/non-O139 (environmental isolates and toxigenic O37 strain ATCC25872) strains. **d,** Retention of plasmids with various origins

Europe PMC Funders Author Manuscripts

of replication in A1552 and three non-O1/non-O139 (SL5Y, SP6G, SA3G) environmental isolates. The different origins of replication (see Methods) were cloned into a neutral plasmid backbone containing a conditional origin of replication inactive in the tested strains. Plasmid stability in **c-d** was determined after growth for approx. 50 generations without antibiotic selection. Bar charts show mean ± sd from three independent experiments (individual dots).

Europe PMC Funders Author Manuscripts

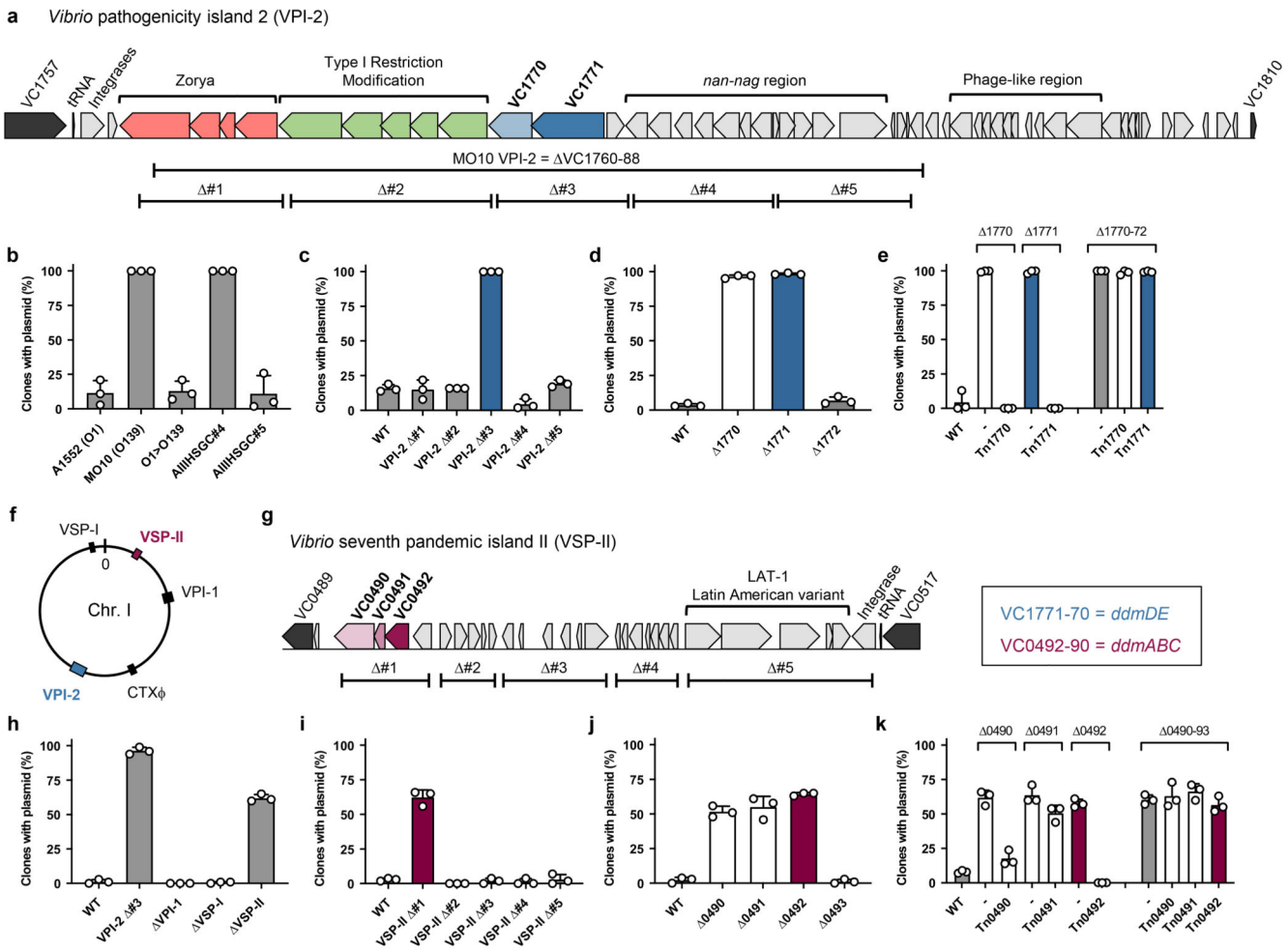

Fig. 2. *V. cholerae* O1 El Tor contains two plasmid defence systems on pathogenicity islands.

a, Schematic showing *Vibrio* pathogenicity island 2 (VPI-2) highlighting the region missing in strain MO10.**b,** pSa5Y-Amp stability in strains A1552 (O1), MO10 (O139), an A1552 transformant with the O1 serogroup exchanged to O139 (O1>O139) and transformants with the O1 serogroup cluster partially exchanged by the O139 region, with (AIIIHSGC#4) and without (AIIIHSGC#5) co-transfer of the truncated version of VPI-2 (ΔVC1760-VC1788). **c,** Effect of deletion of VPI-2 segments missing in MO10 (Δ#1-#5, marked in **a**) on plasmid stability. **d,** Effect of individual deletions of VC1770-VC1772 on plasmid stability. **e,** Expression of VC1770 and VC1771 complements the respective deletion but does not complement the deletion of VC1770-72. **f,** Locations of CTXΦ, VPI-1/-2, and VSP-I/-II on chromosome I of A1552. **g,** Schematic showing *Vibrio* seventh pandemic island (VSP-II) and positions of the deleted segments. **h,** pSa5Y-Amp stability in strain A1552 deleted for VPI-1, VSP-I and VSP-II. **i,** Effect of deletion of VSP-II segments (Δ#1-#5, marked in **g**) on plasmid stability. **j,** Effect of individual deletions of VC0490-VC0493 on plasmid stability. **k,** Expression of VC0490 and VC0492 complements the respective deletion but does not complement the deletion of VC0490-VC0493. Genes were expressed from a chromosomally integrated transposon (Tn) using the arabinose-inducible P_{BAD} promoter. Unless noted otherwise, plasmid retention was evaluated in derivatives of strain A1552,

Europe PMC Funders Author Manuscripts

after growth for approx. 50 generations without antibiotic selection, in either LB or for panels (**e**) and (**k**) LB + 0.2% arabinose. Bar charts show mean ± sd from three independent experiments (individual dots).

Europe PMC Funders Author Manuscripts

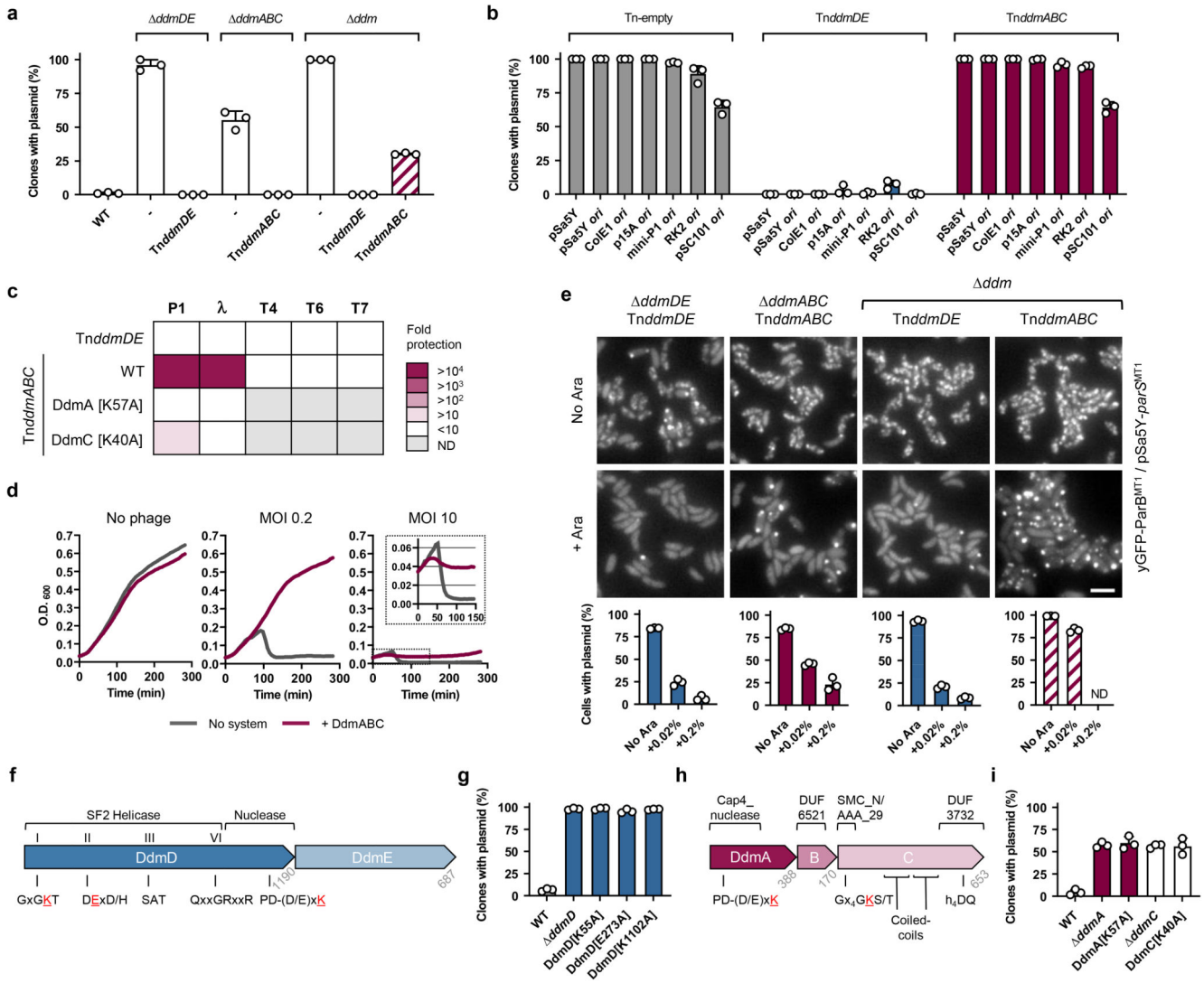

Fig. 3. Mode of action of DdmDE and DdmABC systems.

a, Effect of DdmDE (*TnddmDE*) and DdmABC (Tn*ddmABC*) production on pSa5Y-Amp stability in *V. cholerae*, in the presence and absence of the other system, after growth for approx. 50 generations without antibiotic selection. Δ*ddm* – Δ*ddmDE*Δ*ddmABC*. **b,** Stability of a neutral plasmid backbone utilising various different origins of replication in *E. coli* strain MG1655 bearing either Tn-empty, Tn*ddmDE* or Tn*ddmABC*, after growth for approx. 10 generations without antibiotic selection. **c**, Fold protection against five coliphages conferred by either DdmDE, DdmABC or DdmABC variant production in *E. coli*, as determined by plaque assays. **d**, Growth kinetics of *E. coli* cultures carrying either Tn-empty (No system) or Tn*ddmABC* (+DdmABC) with either no phage or infected at time 0 with phage P1 at MOI 0.2 and 10. Inset shows accelerated lysis of DdmABC-producing culture. Data representative of three independent experiments.**e,** Effect of DdmDE and DdmABC production on pSa5Y-*parS*^{MT1} localisation and retention in *V. cholerae*, in the presence and absence of the other system, after growth for approx. 10 generations without antibiotic selection. Charts below images show quantified plasmid retention. Images representative

Europe PMC Funders Author Manuscripts

of three independent experiments. Scale bar = 2.5 μm. **f-i**, Schematics showing conserved domains and features identified in DdmDE (**f**) and DdmABC (**h**). Residues targeted by site-directed mutagenesis are highlighted in red. Numbers at boundaries indicate protein size (aa). Retention of pSa5Y-Amp in *V. cholerae* strains encoding variants of DdmD (**g**), DdmA and DdmC (**i**) was evaluated after growth for approx. 50 generations without antibiotic selection. Bar charts show mean ± sd from three independent experiments (individual dots). ND, not determined. Genes in panels (**a-e**) were expressed from a chromosomally integrated transposon (Tn) using the arabinose-inducible P_{BAD} promoter. Growth media were supplemented with 0.2% arabinose, except for Tn*ddmABC* in the presence of plasmids, which used 0.02% arabinose due to toxicity.

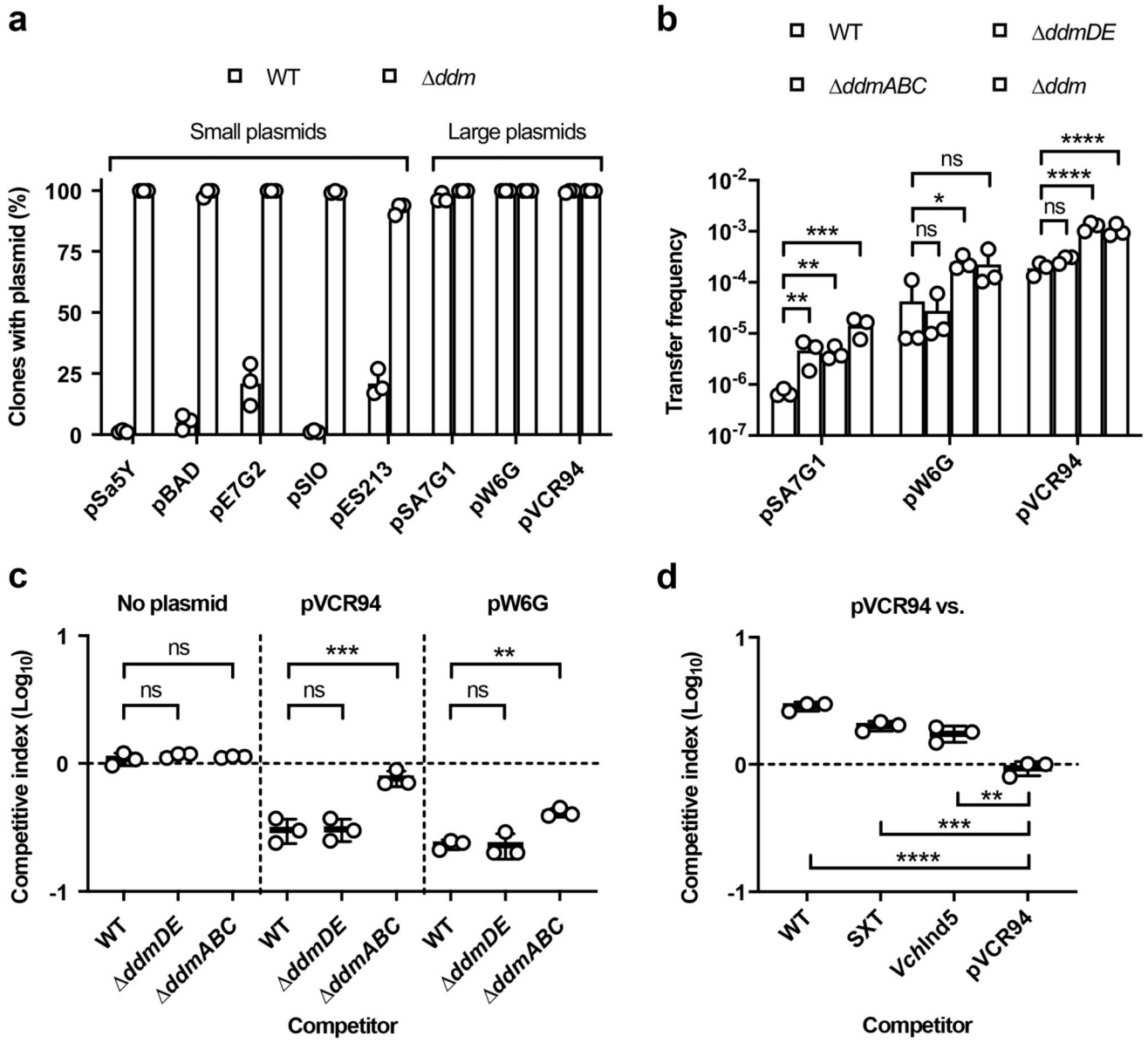

Fig. 4. Impact of DdmDE and DdmABC systems on *V. cholerae* 7PET ecology.

a, Retention of small (<10kb) and large (pSA7G1, 79.4kb; pW6G, 306.5kb; pVCR94, 171.8kb) plasmids native to *V. cholerae, V. fischeri* (pES213) or *E. coli* (pBAD) evaluated in A1552 (WT) and Δ*ddm (ΔddmDE ΔddmABC*) after growth for approx. 50 generations without antibiotic selection. Plasmids contain an added kanamycin resistance cassette for quantification, except pVCR94, for which natural ampicillin resistance was used. **b,** Conjugation assay showing the transfer frequency of the large plasmids into A1552 and derivative strains. **c-d,** Co-culture experiments evaluating competition between the indicated strains after growth for approx. 50 generations without antibiotic selection. **c,** Competitive index of strains A1552 (WT), Δ*ddmDE* and Δ*ddmABC* carrying either no plasmid, pVCR94 or pW6G, competed against A1552Δ*lacZ*. **d,** Competitive index of strains A1552 (WT),

A1552-SXT, A1552-*Vch*Ind5 and A1552 carrying pVCR94, competed against *A1552ΔlacZ* carrying pVCR94. Data represent mean ± sd from three independent experiments (individual dots). Significant differences were determined by one-way ANOVA with either Dunnett's (**b** and **c**) or Tukey's (**d**) post-test. *$P < 0.05$; **$P < 0.01$; ***$P < 0.001$; ****$P < 0.0001$; ns – not significant.

Europe PMC Funders Author Manuscripts